CALIFORNIA STATE UNIVERSITY, NORTHRIDGE

PALEOSEISMIC INVESTIGATION OF THE SAN GORGONIO PASS FAULT ZONE NEAR CABAZON, CALIFORNIA

A thesis submitted in partial fulfillment of the requirements
For the degree of Master of Science
in Geology

By

Shahid Ramzan

August 2012

The thesis of Shahid Ramzan is approved:

_____	_____
Vicki Pedone, Ph.D	Date
_____	_____
Richard Heermance, Ph.D	Date
_____	_____
J. Douglas Yule, Ph.D. Chair	Date

California State University, Northridge

DEDICATION

My efforts for this thesis are dedicated to:

my parents for their love and encouragement

my wife Samyya and daughter Ayesha for their patience and support throughout graduate school.

ACKNOWLEDGEMENTS

I am very much obliged to my thesis advisor, Dr. Doug Yule, for his advisement and friendship throughout this project. A very heartfelt thanks to Paul McBurnett for help with trenching, cleaning and also for introducing me to the experience of trenching during the hottest days of California. I would like to thank the Morongo Mission Band of Indians for graciously allowing us to trench and do research on their lands and to Lonnie Rodriquez, James Payne, and Liz Bogdanski of the Morongo Tribe's Environmental Department. Thanks also goes to the trench party participants to review my work, Katherine Kendrick, Sinan Akciz, Kate Sharer, Tom Fumal, Jerry Treiman, and John Tinsley. Your invaluable input to my thesis is greatly appreciated especially about the curious burrow structure. I would also like to send my sincere thanks to Christopher Madden, a fellow graduate student at Oregon State University for introducing me to paleoseismology. I am also grateful to my other committee members, Dr. Vicki Pedone and Dr Richard Heermance for their valuable comments and suggestions regarding early draft of this document. In addition, thanks to Mike Tacsik for saving my hours whenever I was stuck working with Adobe Illustrator® and Photoshop®.

TABLE OF CONTENTS

LIST OF ILLUSTRATIONS

Page

LIST OF TABLES

List of plates

ABSTRACT

PALEOSEISMIC INVESTIGATION OF THE
SAN GORGONIO PASS FAULT ZONE
NEAR CABAZON, CALIFORNIA

By

Shahid Ramzan

Master of Science in Geology

The discontinuous nature of the San Andreas fault at San Gorgonio Pass has led to competing models about whether or not large earthquakes can rupture through this structurally complex region. To test these models I excavated trenches across the San Gorgonio Pass fault zone (SGPFZ) near Cabazon as part of a larger effort. The trench site is located ~100 m to the east of a site excavated in 1997 by Yule where trenches uncovered evidence for at least one earthquake 500-700 yrs ago. At the 1997 site extensive bioturbation and low sedimentation rates hampered efforts to distinguish events. The new site, located where two alluvial fans merge, was selected for its higher sedimentation rates and excellent stratigraphy. Excavations at the new site contain incipient soil layers that subdivide the stratigraphy into six units (Units 100 to 600, from base to top of the section). The units form tabular to wedge-shaped layers up to ~1 m thick. In general, the base of each unit consists of yellowish-gray, thin- to medium-bedded sand and pebbly sand, with occasional gravel lenses and mud and silt interlayers. The tops of each unit are more massive; they locally contain numerous burrows and display a slight orange-red oxidized soil horizon. A distinct angular unconformity lies at

the base of Unit 400. Units that underlie the unconformity (100-300) are cut by a fault that strikes N35-50° E and dips 15-30° NW. The fault shows 1.0 to 1.5 m of vertical separation, equivalent to 2.5 to 6 m of slip resolved parallel to a N45°W slip vector. Unit 400 is up to 1 m thick at the south end of the trench and pinches out against the fault scarp on the north. A channel fill sequence in Unit 500 caps the scarp. The stratigraphic (onlap) and structural (faulting) relations clearly restrict the most recent event (MRE) to have occurred post- and pre-deposition of Units 300 and 400, respectively. Radiocarbon ages from detrital charcoal fragments constrain the timing of this earthquake to between ~600-800 yrs BP. I suspect that the story here is incomplete because, due to a road that I could not excavate, I did not extend the trenches across the entire fault zone. However, results from this and a 1997 study led by D.Yule (which trenched the complete fault zone) suggest that the most recent earthquake occurred 600-700 yrs BP. Evidence from Cabazon therefore supports a model with infrequent ruptures (by San Andreas fault standards) in San Gorgonio Pass and rare through-going events.

INTRODUCTION

The structural complexity and diffuse seismicity of the San Gorgonio Pass region has led to competing views about the types of earthquakes that can occur here (Allen, 1957; Matti et al., 1985; Jones, et al., 1986; Matti and Morton, 1993; Seeber and Armbruster, 1995; Magistrale and Sanders, 1996; Yule and Sieh, 2003; Langenheim et al., 2005). At one extreme the ShakeOut Scenario earthquake (Jones et al., 2008) depicts a M7.8 earthquake that ruptures through the structural complexity of San Gorgonio Pass. An alternative view argues that the complexity in the Pass region inhibits through going ruptures and limits their size to <M7.5 (Sykes and Seeber, 1985; Carena et al., 2004; Langenheim et al., 2005).

Northwest-striking strike-slip faults of the San Andreas fault system feed into San Gorgonio Pass from either direction, the San Bernardino strand of the San Andreas fault on the northwest and the Coachella Valley strand of the Banning fault from the southeast, but appear to end as they approach the east-west striking fold and thrust belt of the San Gorgonio Pass fault zone (Figure 1). Oblique-normal faulting on the Cox Ranch and related faults also occurs here but is interpreted to be a second-order feature related to the steepening of the north dipping San Gorgonio Pass fault zone at depth (Yule and Sieh, 2003) (Figure 2). The 15-km-long segment of the San Gorgonio Pass fault zone, therefore, appears to cut across the San Andreas fault system and contains the San Bernardino strand in its hanging wall. The competing models mentioned above are in general agreement with this geometry but disagree on the role that the San Gorgonio Pass fault zone plays during large San Andreas earthquakes here.

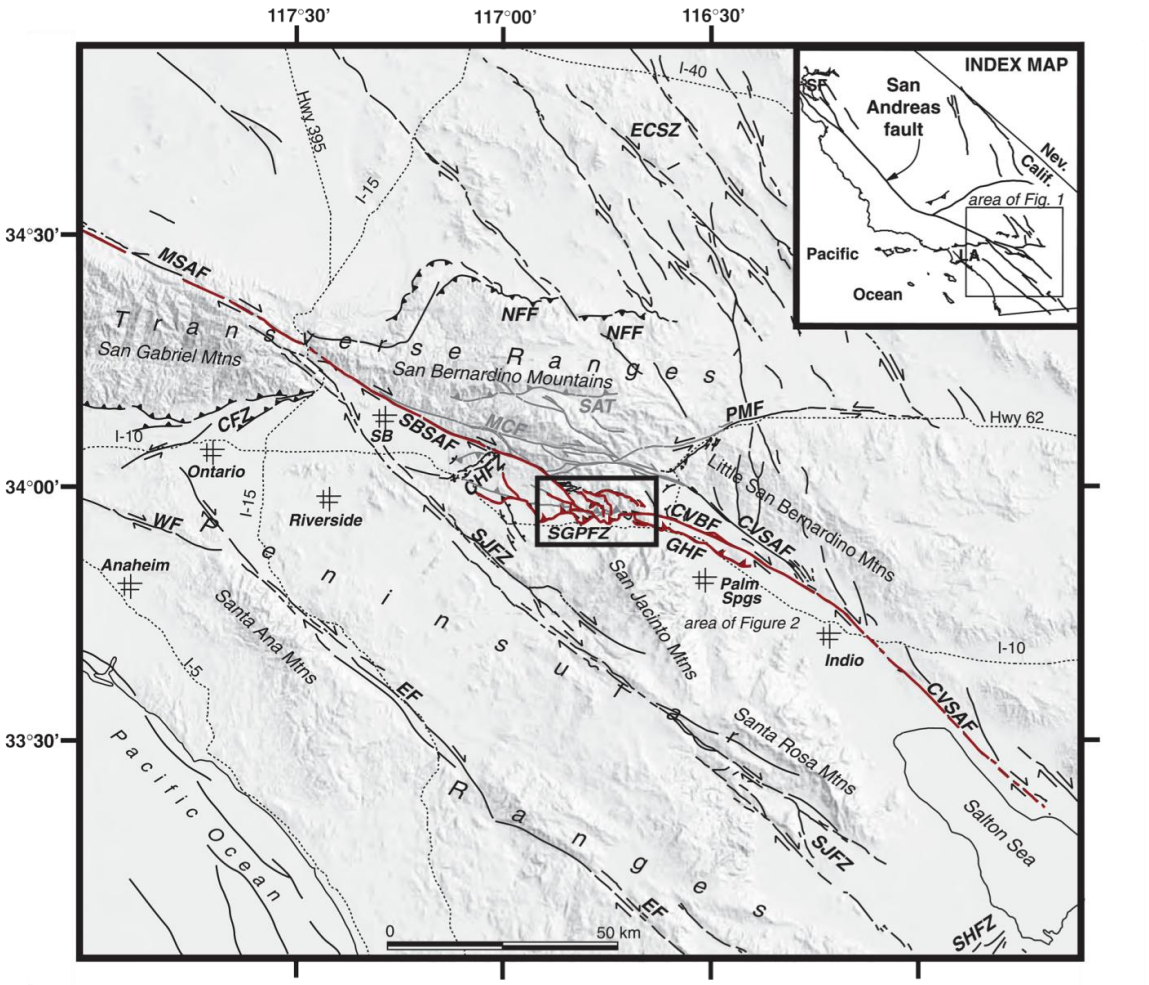

Figure 1. Shaded topographic relief map of the eastern Transverse Ranges and northern Peninsular Ranges, southern California, showing Holocene faults in black. Late Pleistocene faults in the vicinity of San Gorgonio Pass, considered inactive, in gray. Abbreviations: CFZ, Cucamonga fault zone; CHFZ, Crafton Hills fault zone; CVBF, Coachella Valley strand Banning fault; CVSAF, Coachella Valley strand, San Andreas fault; EF, Elsinore fault; ECSZ, eastern California shear zone; GHF, Garnet Hill fault; MCF, Mill Creek fault; MSAF, Mojave strand, San Andreas fault; NFF, north frontal fault; PMF, Pinto Mountain fault; SAT, Santa Ana thrust; SBSAF, San Bernardino strand, San Andreas fault; SGPFZ, San Gorgonio Pass fault zone; SHFZ, Superstition Hills fault zone; SJFZ, San Jacinto fault zone; and WF, Whittier fault; SB, San Bernardino; LA, Los Angeles; SF, San Francisco. Modified from Yule and Sieh (2003).

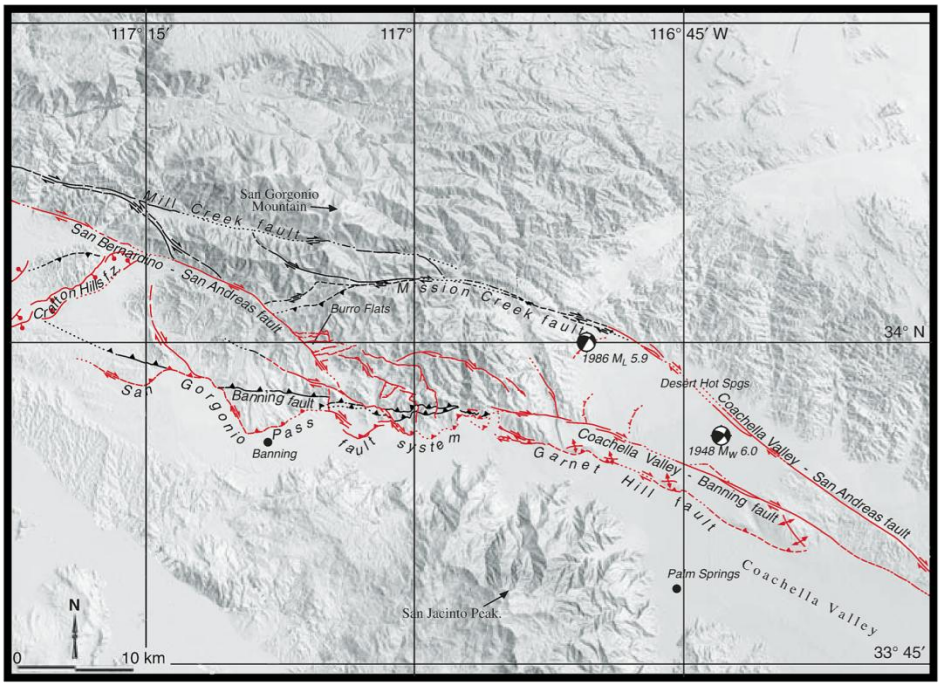

Figure 2. From Yule (2009). Shaded-relief topographic map of San Gorgonio Pass region shows traces of active faults in red, inactive faults in black. Mapping from Allen (1957), Matti et al. (1985), and Yule and Sieh (2003). First-motion diagrams show epicenters of moderate earthquakes that have struck the region since 1948.

Two end-member hypotheses exist to attempt to explain possible scenarios of large earthquake behavior involving the San Gorgonio Pass fault zone. The through-going model suggests a rupture of M 7.8 from the Salton Trough to the Mojave Desert, whereas the barrier model forecasts a < M 7.5 event that is arrested by the complexities of the San Gorgonio Pass fault zone. Models such as the ShakeOut scenario earthquake (inset of Figure 3) use a through-going rupture model as a worst-case scenario for earthquake hazards facing southern California.

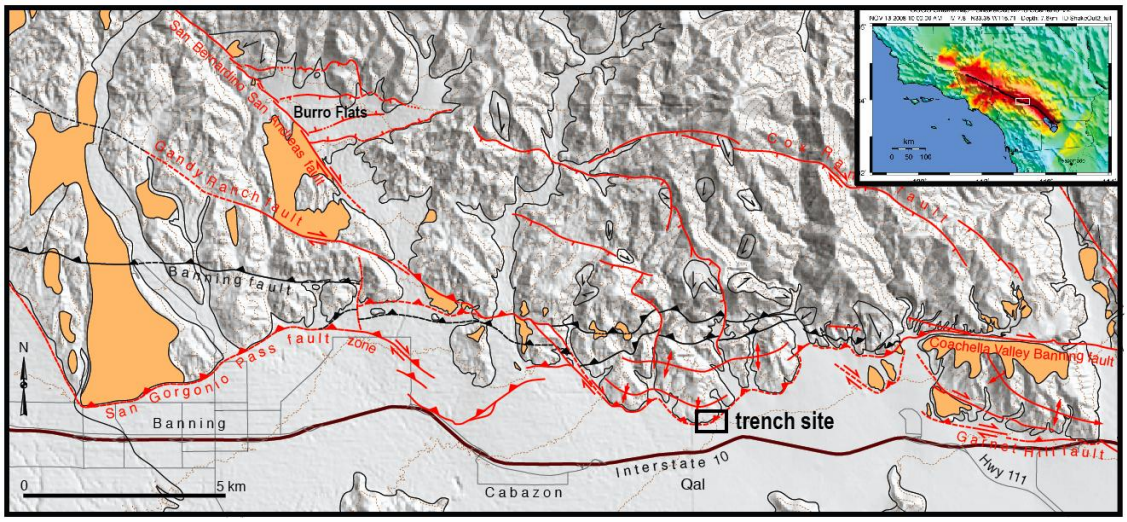

Figure 3. Fault map of the central San Gorgonio Pass region with active faults shown in red and inactive faults in black. Up-on-the-north scarps are common along the San Gorgonio Pass fault zone to the north of Interstate 10. Boxed area to the north of Interstate 10 locates the Cabazon trench site described in this thesis. Barbs indicate up thrown sides of thrusts, tick marks indicate downthrown sides of normal faults; arrows show relative sense of strike-slip motion. Remnants of late Pleistocene strath terraces are shown in light orange. **Inset**: USGS ShakeOut Scenario **M** 7.8 earthquake for rupture along the southern San Andreas fault. Red color indicates areas of the most intense ground shaking. White box is centered on the San Gorgonio Pass region.

This thesis documents a paleoseismic investigation conducted across the San Gorgonio Pass fault zone at a site located approximately 1.6 km north of the town of Cabazon, California (black boxed area in Figure 3). This investigation included excavation and detailed logging of two trenches, photographic documentation of trenches, radiocarbon analysis, and data interpretation. The purpose of this study is to expand the understanding of the behavior of seismic activity on San Gorgonio Pass fault zone during the large earthquake.

My thesis seeks to answer the question: is through-going San Andreas fault rupture possible? And if so, how often does this type of quake occur? The data from my study at Cabazon, when added to previous San Andreas quake correlation diagrams (e.g., Philibosian et al., 2011), show that large, through-going ruptures are relatively infrequent San Andreas events.

GEOLOGIC AND TECTONIC SETTING

Bedrock units of San Gorgonio Pass region comprise three terranes: the San Bernardino Mountains, San Gabriel Mountains, and Peninsular Ranges. A possible fourth type of terrane present in the southeastern part of the San Gabriel Mountains has been correlated with Peninsular Ranges rock (Matti et al., 1985). The Peninsular Ranges terranes are further divided into mafic western and felsic eastern parts distinguished by lithological differences in both prebatholithic and batholithic rocks (Langenheim et al., 2005). San Gabriel Mountains terrane is separated into two units by the Vincent thrust, which places various upper-plate Mesozoic plutons and prebatholithic rocks on top of lower-plate Pelona Schist. The San Bernardino Mountain terrane is composed of basement rocks similar to those in the western Mojave Desert and consists of three major rock types: (1) gneiss and granitoids of various types (2) sedimentary rocks of the Cordilleran miogeocline, and (3) Permian and Mesozoic plutons (Langenheim et al., 2005). Sedimentary rocks include Neogene strata that form a wedge separating the San Gabriel and Peninsular Ranges terranes. The strata are exposed in the hanging wall of the San Gorgonio Pass fault zone. They include the Miocene marine Imperial Formation and non-marine Painted Hill, Hathaway, and Cabazon Formations.

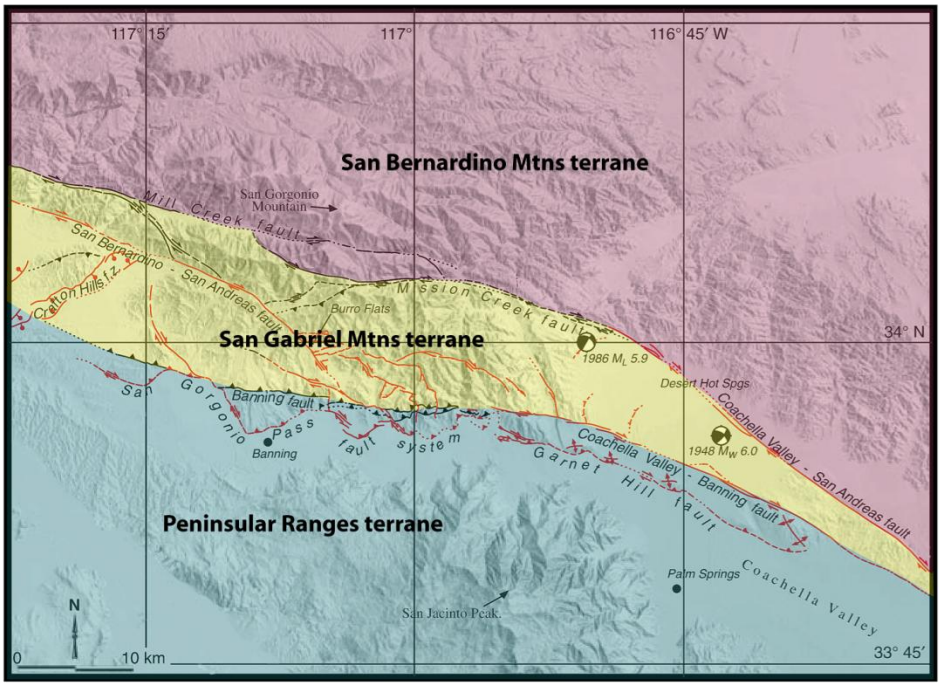

Figure 4. Modified figure from Yule (2009). Shaded-relief topographic map of San Gorgonio Pass (SGP) region shows Bernardino Mountains, San Gabriel Mountains, and Peninsular Ranges terranes.

Fault Geometries

To the northwest of San Gorgonio Pass, the San Andreas fault system consists of two main splays, the active San Bernardino strand and the inactive Mill Creek strand (Figure 2). To the southeast of the Pass, the San Andreas consists of three main splays: the Mission Creek, Banning, and Garnet Hill strands. Notably, the San Bernardino and Banning strands do not connect at the surface but instead appear to merge with the thrust-dominated San Gorgonio Pass fault zone.

Three main hypotheses have been put forth to attempt to explain the complex faulting relationships within the San Gorgonio Pass. Rasmussen and Reeder (1986) suggest a mega-landslide has cut off the San Andreas fault at depth. Using strike-slip focal mechanisms, Seeber and Armbruster (1995) conclude that the vertical San Andreas

fault is continuous at depth but displays active thrusting at the surface. The third hypothesis suggests the San Gorgonio Pass fault zone transfers dextral slip through a series of discontinuous strike-slip and thrust faults as suggested by Matti et al. (1985, 1992a) and Matti and Morton (1993). Yule and Sieh (2003) argue against Rasmussen and Reeder (1986) and Seeber and Armbruster (1995) and favor the third model. Results from Rasmussen and Reeder (1986) and Seeber and Armbruster (1995) are also disputed by results from Carena et al. (2004). This study of subsurface seismic fault geometries shows a north 50° - 80° dipping fault plane beneath San Gorgonio fault zone with no evidence of a vertical San Andreas fault. Carena et al. (2004) also conclude that the Pass region is a system of 60 complex strike-slip and reverse faults that will rupture in a complex way if a through-going rupture occurs.

Active and Inactive Faults

Active structures mapped by Vaughan (1922), Lawson et al. (1908), Allen (1957), Matti et al. (1985, 1992a), Matti and Morton (1993), and Yule and Sieh (2003) show Holocene movement on faults within the San Gorgonio Pass (Figures 2 and 3). Active branches of the San Andreas fault show recent activity in Holocene alluvium, terrace risers, or deformed Holocene units (Yule and Sieh, 2003). Faults within the Pass region may have active and inactive sections on the same strand. The Banning strand enters the San Gorgonio Pass as a strike-slip fault, begins to dip to the north, and becomes the San Gorgonio Pass thrust. This segment of the Banning strand feeds into an inactive and active fault segment that continue west into the Pass. Near the Cabazon trench site the active fault turns north northwest and becomes strike-slip again as it merges and reactivates the Banning fault, now inactive along most of its trace. At this point the thrust

fault shows signs of recent activity in Millard Canyon and contains a scarp that cuts Holocene alluvium. The Gandy Ranch Fault is another fault that appears to be active in places, inactive in others. For example, a fault scarp in young alluvium and offset ridgelines are present between Potrero and Hathaway Canyons, but signs of recent motion are not evident to the west.

Slip Rates and Recurrence Intervals

South of the Cajon Pass, the San Andreas fault disaggregates into a broad zone of deformation (Yule and Sieh, 2003) and the North American/Pacific Plate Boundary becomes more diffuse. A family of faults occupies this diffuse zone including the Elsinore fault, San Jacinto fault, and Eastern California Shear Zone. The San Andreas fault is the primary structure with slip rates of 15–35 mm/yr and earthquake recurrences of 100–200 years (Table 1, and references therein).

GPS studies are in agreement with geologic studies. Becker et al (2005), using GPS velocity and stress inversions, determined geodetic slip rates of 15-18 mm/yr for the Eastern California Shear Zone, 15 mm/yr for the San Jacinto fault, and 23 mm/yr for the Indio strand of the San Andreas fault. These rates agree with the geologic slip rates south of Cajon Pass on individual faulting systems. Recurrence intervals also reflect this distribution of stress on the San Andreas fault. (Table 1, and references therein).

Table 1			
Slip Rates and Recurrence Intervals for the San Andreas Fault System			
From Parkfield Continuing South to Salton Trough			
Reference	Site	Average Recurrence(yrs)	Slip Rates
Toke et al. (2011)	Parkfield		~26.0
Young et al. (2002)	Cholame	290-410	
WGCEP	Cholame	~140	34±5
Stone et al. (2002)	Cholame	236	
WGCEP	Wallace Creek		~35
Noriega et al. (2006)	Van Matre Ranch		29.3-35.6
Akciz et al. (2009)	Bidart Fan	137±44	
Grant and Sieh (1994)	Bidart Fan	156	
Biasi et al. (2002)	Pallet Creek	135	
Fumal et al. (2002)	Wrightwood	105	
Weldon et al. (2002)	Wrightwood		20-40
Scharer et al. (2007)	Wrightwood	111-123	
Weldon and Sieh (1985)	Cajon Pass		24.5-3.5
McGill et al. (2007)	Badger Canyon		11-16
Fumal et al. (2002)	Thousand Palms	215±25	4±2
McGill et al. (2006)	Plunge Creek		3-17
Shifflett et al. (2002)	Mecca Hills	260±100	12 and 5-8
Behr et al. (2010)	Biskra Palms		11-22
Keller et al. (1982)	Biskra Palms		10-35
Van der Woerd et al. (2006)	Biskra Palms		15.9±3.4
Philibosian et al. (2011)	Lake Cahuilla	180	
Yule et al. (2001)	Garnet Hill		5.7±0.8
Orozco (2004)	Burro Flats		2.6-7.0
Matti et al. (1992a)	Millard Canyon		1-1.3*
Yule and Sieh (2003)	San Gorgonio Pass		5*
McBurnett (2011)	Millard Canyon	471-540	3.0-6*
This Study	Lion Canyon	600-700	
Yule and Sieh (2001)	Burro Flats	300	
Becker et al. (2004)	GPS		23±8
Bennet et al. (1996)	GPS		22±2

Table 1. Published slip rates and recurrence intervals for the San Andreas fault system south of Parkfield, CA. Note the overall decrease in velocities and recurrence intervals south of the Cajon Pass demarked by the bold orange line. Geodetic data are significantly higher than geologic rates for the southern San Andreas fault system.

* Uplift or partial uplift rates

In the San Gorgonio Pass region, uplift plays a significant role in conjunction with dextral components of slip (Cooke et al., 2011 and Spotila et al., 1998). Strike-slip movement of the San Andreas fault decreases as it enters the San Gorgonio Pass and thrust faulting begins to become a major component of the faulting in the Pass (Yule and Sieh, 2003). Here, the igneous-metamorphic rocks of the San Bernardino Mountains are thrust over Neogene strata and crystalline rocks of the San Jacinto Mountains.

Recent studies at Millard Canyon (McBurnett, 2011) constrain the San Andreas fault's rupture history in San Gorgonio Pass. At the Millard Canyon trench site two ruptures have occurred in last ~1300 years, one at ~700 years BP and one at ~1200 years BP. Previous studies at Cabazon (Yule et al., 1997) also constrain the timing of most recent event <707 years BP. Therefore Millard Canyon and Cabazon studies supports a model with relatively infrequent ruptures (by San Andreas fault standards) in San Gorgonio Pass that are probable through-going San Andreas events.

GEOMORPHOLOGY OF CABAZON TRENCH SITE

Two trenches located on the western margin of Lion Canyon fan were excavated at the Cabazon site (Figures 3 and 5) for this study. Trenches excavated in 1997 (T1-4), show that several zones of thrust faulting occur over a 20 m-wide zone (Figure 6). The southernmost of these fault zones was unearthed in the 2011 excavation for this study, in the NW end of the Trench 5. This fault is buried at the site by sediment derived from Lion Canyon (Figure 6). I mapped geomorphic surfaces using topographic relations and soils to establish the boundaries of units. I discovered a gentle scarp trending E-W and defined five tectonic geomorphologic map units (Figure 6).

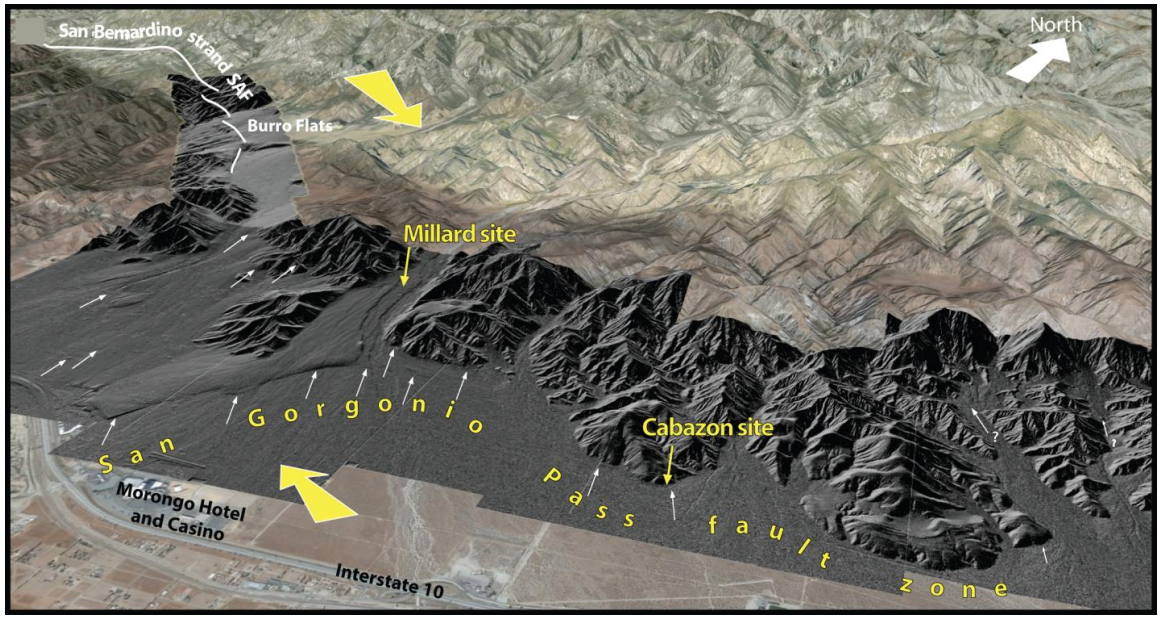

Figure 5. Oblique view looking northwest above the central San Gorgonio Pass region. DEMS are prepared from B4 LiDAR data and draped over Google Earth Imagery. Thick yellow arrows approximate the relative motion between the San Jacinto and San Gorgonio Mountains blocks on either side of the active fault zones. The dextral strike-slip San Bernardino segment of the San Andreas fault enters the imaged area in the upper left at Burro Flats. White arrows point at Holocene fault scarps along the San Gorgonio Pass fault zone, an active, oblique thrust fault system that transfers slip through the Pass to the east into Coachella Valley where right-lateral strike-slip motion again predominates. The Cabazon (this study) and Millard (McBurnett, 2011) trench sites are located at the tips of the thin yellow arrows.

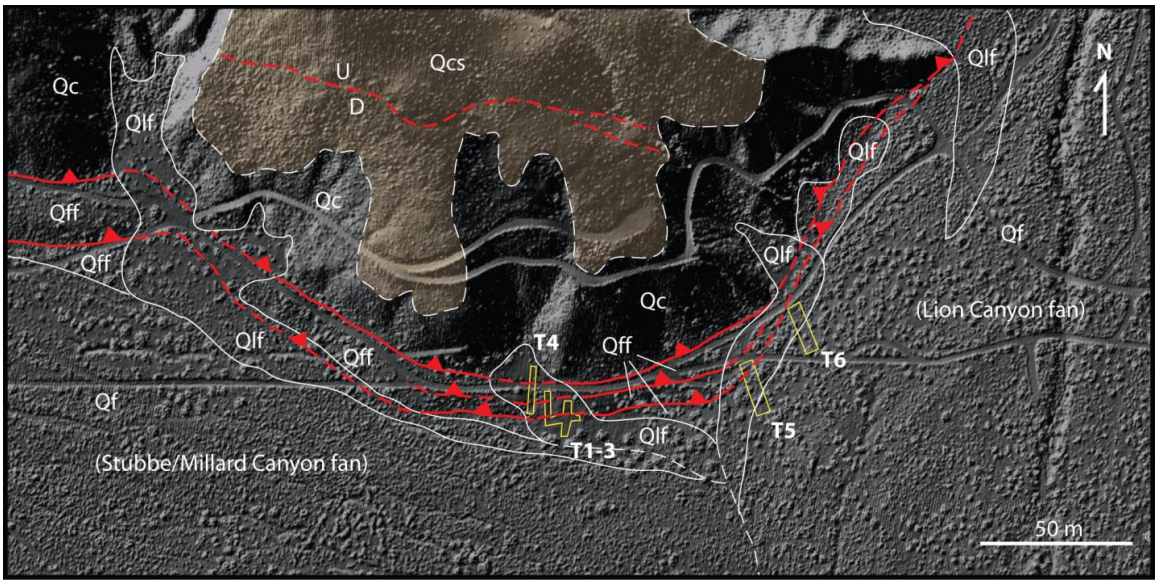

Figure 6. Tectonic geomorphologic map of the Cabazon trench site. DEM is from B4 LiDAR data. A total of six trenches have been excavated here (in yellow), T1-4 in 1997 and T5-6 in 2011. Qc = Pleistocene Cabezon Formation (fanglomerates); Qcs = relatively low-relief surface with well-developed, orange-red soil developed in Cabazon Formation gravels; Qff - faulted fan gravel; Qf = alluvial fan gravels of Stubbe/Millard and Lion Canyons; Qlf = local fans and colluvium.

METHODOLOGY

The objective of this study was to constrain the size and timing of the most recent rupture on the San Gorgonio Pass by excavating a paleoseismic trenches across the fault scarp. The trench locations for my study (Trench 5 and Trench 6) were selected to try and improve upon previous work at a nearby site (Yule et al., 1997) that documents a complex zone of late Holocene thrust faulting but has relatively poor age control and low sedimentation rates. Trenches 5 and 6 for this study are located on the western margin of Lion Canyon fan (Figure 6). Here the scarp is buried indicating high sedimentation rates. Furthermore, the relatively large drainage basin of Lion Canyon enhances the likelihood for abundant detrital charcoal. In addition, Trenches 5 and 6 are easily accessible along a series of power line roads. I was unable to gain permission to excavate across the roads; a reality that prevented Trenches 5 and 6 from extending north across the roads and into the hillslope (Figure 6). After these trenches were excavated and logged, a mini-trench was dug to confirm lateral extent of specific features observed in Trench 5. My field assistants and I manually excavated a 0.5-m-deep and 6-m-long trench in east wall of Trench 5. The purposes of this mini trench were to confirm the fault zone in upper wall and to provide a 3D view of the fault. Appendix A gives the results, trench log and images from this excavation.

Excavation

Trenches 5 and 6 were excavated by backhoe in January of 2011 (Figure 7), perpendicular to the projected fault scarp (Figures 6, 7, and 8). The trenches were extended to 22 m and 21 m lengths respectively, at a maximum depth of about 3 m. The length for both trenches was limited due to the existing roads. Trench 5 was located ~100 m to the east of a site excavated in 1997 by Yule. Trench 6 was located ~50 m to the NE from Trench 5 (Figures 6 and 8). Trench 6 did not expose any fault and therefore places limits on the fault's location, probably to a narrow zone between the northwest end of Trench 6 and the base of the hill (Figure 8).

Figure 7. Start of Trench 5 excavation at Cabazon, January 3, 2011

Figure 8. View to the southeast across trench site (San Jacinto Peak with snow in distance). Trench 5 is located to the south of truck and Trench 6 is located ~50 m to the east, between the two roads, where excavator is digging at south end of Trench 6. Solid and dashed lines show position of thrust zone (on either side of the truck). Sawteeth are placed on the hanging wall. Thrust faults are exposed in north end of Trench 5; no faulting was exposed in Trench 6 (thrust presumed to lie beneath dirt road to the north of Trench 6).

Trench Wall Preparation and Logging

After excavation the trench walls were scraped clean and smooth to provide an enhanced view of the stratigraphy and the structural relationships of the layers. Following the cleaning of the walls of the trenches, a string grid (0.5 m ×1.0 m) was set up on each trench wall and held in place by nails. Distinct strata were marked with different colored nails. Photographs of the trench walls were taken as an archive of the trench walls. Additional close-up photos were taken at key structures and contacts. Photo mosaics of

the two walls in Trench 5 and one wall of Trench 6 (both walls were identical) were then created with Adobe Photoshop, version CS3. Mosaics provided a base for initial logging and unit interpretation. Detailed logs for the both trenches were also made on grid paper for each trench wall at the scale of 1:20 (Plates 1 and 2). The logs provide a detailed record of what was observed on the trench walls. Finally digital productions of logs were compiled in Adobe Illustrator CS3, version (Plates 1 and 2). Samples of detrital charcoal were collected to determine ages of the stratigraphic units and fault, and their locations were recorded on the logs.

Radiocarbon Dating

The ^{14}C method of dating is based on measurements of the activity of ^{14}C in carbon-bearing materials that originally were in communication with CO_2 gas of the atmosphere. ^{14}C is produced in the atmosphere by the interactions of cosmic-ray produced neutrons with stable isotopes of nitrogen, oxygen, and carbon. The most important of these is the reaction between slow cosmic-ray neutrons and the nucleus of stable ^{14}N. When plant material dies, the absorption of ^{14}C from the atmosphere stops; and the activity of ^{14}C then declines as a result of radioactive decay. If the activity of ^{14}C in living tissues is known, the activity of ^{14}C of dead plant tissues can be used to calculate the time elapsed since death.

The strata at the Cabazon site contain abundant detrital charcoal. A total of 102 samples were collected in glass vials. We evaluated the samples based on size and location relative to deformation selecting 37 samples for analysis. A first set of 5 samples was processed at the University of California, Irvine, Keck Carbon Cycle Accelerator Mass Spectrometry, and a second set of 21 samples was sent to Lawrence Livermore

National Laboratory (LLNL) in Livermore, California. The laboratory results were calibrated to calendar years using OxCal v.4.0.1 (Bronk Ramsey, 2009). The locations of the dated charcoal samples are shown on the trench logs (Plate 1). A third set of 12 samples was also processed at Lawrence Livermore National Laboratory (LLNL) in Livermore, California. In addition, we collected four bulk samples of organic material for Unit 300 and Unit 400 (Figure 9).

As part of a separate study, five Optically Stimulated Luminescence samples were collected from west wall of Trench 5 by Katherine Kendrick of United States Geological Survey. Details about the locations where and how the samples were collected are provided in Appendix B.

Figure 9. Photo of a bulk radiocarbon sample taken from Unit 300, west wall of Trench 5, meter 9 west (9W).

Figure 10. Photo from west wall of Trench 5 showing organic-rich (peaty?) layer deposited during a time of relatively little clastic sediment deposition (or fast vegetation growth and soil development). Laminated medium sand layer buries organic layer, in turn overlain by massive medium to coarse sand (photograph is ~10cm×25cm).

Figure 11. Photo from west wall of Trench 5 showing thin, dark organic-rich layers (above horizontal string grid) and interlayers of laminated fine sand and massive medium to coarse sand (Scraper is 15cm long).

STRATIGRAPHY

The stratigraphic units exposed in Trenches 5 and 6 contain variable amounts of: 1) massive sand, muddy sand, and pebbly, muddy sand; 2) laminated fine to corse sand, with local pebble-rich sand; 3) pebble to cobble gravel and sandy gravel: and 4) thin organic-rich mud layers. Also occasional lamination and cross bedding is preserved krotovina (back-filled burrows) are locally abundant. In addition, abundant roots and rootlets occur in the uppermost 0.5 m of the Unit 600. Massive layers commonly cap each unit and have a light-organic color that is interpreted either as an or due to an influx of orange clay from a deeply weathered soil developed on a Cabazon Formation gravel in the hill to the north.

The poorly sorted sand and gravel dominated sediments are typical of alluvial fan deposits. The massive, poorly sorted mud-sand-gravel deposits likely formed by debris flows; whereas the sand-dominated units represent smaller storm events and/or reworking of older fan deposits by stream flow. The organic-rich, silty, muddy sand units likely formed in marshy, vegetated swales on the fan surface.

I divided the trench stratigraphy into 6 stratigraphic units, Units 100 to 600, based on lithological characteristics, distribution, and stratigraphic relations (Tables 3 and 4). The top of each unit is characterized by a distinct, orange-to brown-orange-weathering, massive (soil?) layer. Units 100 to 600 are present in Trench 5, and Units 200 to 600 are present in Trench 6. The trench logs in Plate 1 and Plate 2 show the stratigraphic relationships of the units. All units in both trenches are laterally continuous except Unit 500 on the west wall of Trench 5. Here, the typical yellowish-gray, pebbly, muddy sand, is truncated by two lenticular units of grayish brown pebbly, muddy sand, Units 500b and

500c (Figure 13). The percentage of gravel and the clast sizes in these units are greater than those in Unit 500a. The erosional lower contacts, bed geometry, and large clast size indicate that these units are channel deposits. Unit 500c truncates Units 500a and 500b, indicating a second and younger episode of erosion and fill than that of Unit 500b.

Table 2 Stratigraphy of Trench 5 and Trench 6

Location	Unit	Maximum thickness	Lithologic description	Interpretation	Trench 5	Trench 6
Cabazon-T 5	600	0.5 m	Fine to medium-grained, massive, medium to dark gray, bioturbated with rootlets, yellow-brown silty sand with some pebbles	Fluvial sand and gravel with some thin organic-rich muddy layers	**X**	**X**
Cabazon-T 5	500a	0.8 m	Fine to coarse-grained, massive, yellowish-gray thin to medium bedded, interbedded silty mud, fine to coarse gravel, pebbly muddy sand	Interlayered massive debris flow and fluvial layers	**X**	**X**
Cabazon-T 5	500b	1 m	Fine to coarse-grained, massive fine to coarse fluvial gravel that fills channel incision into 500a, grayish-brown, pebbly muddy sand	Channel fill	**X**	**X**
Cabazon-T 5	500c	0.8m	Fine to coarse-grained, massive fine to coarse fluvial gravel that fills channel incision into 500b, grayish-brown, pebbly muddy sand	Channel fill	**X**	**X**
Cabazon-T 5	400	1 m	Fine sand with scattered coarse sand, massive, interbedded with clayey silt layers, dark gray, clayey sand	Interlayered massive debris flow and fluvial sand layers	**X**	**X**

Cabazon-T 5	300	0.7 m	Fine to coarse-grained, massive, yellowish-gray, pebbly muddy sand	Intebedded massive debris flow and secondary fluvial layers	**X**	**X**
Cabazon-T 5	200	0.6 m	Fine to coarse-grained, massive, occasional discontinuous silty muddy layers, yellowish-gray, muddy sand	Intebedded massive debris flow and secondary fluvial layers	**X**	**X**
Cabazon-T 5	100	0.5 m	Fine to coarse-grained, massive, yellowish-gray, pebbly sand	Intebedded massive debris flow and secondary fluvial layers	**X**	

STRUCTURES AND ANGULAR UNCONFORMITIES

Both the east and west wall of the northern end of Trench 5 expose a main fault zone with several splays that cut Units 100-300 (Figure 12; Plate 1). No structures were observed in Trench 6 (Plate 2). Faults in Trench 5 strike N35°-50°E and dip 15°-30°NW. A single fault at the bottom of the trench meter 2 (Plate 1) splays upward into two main splays (Plate 1; Figures 12, 13, and 14). Vertical separation across the fault zone here is ~0.75-1.0 m on the top of Unit 100, and ~0.5-0.75 m on the top of Unit 200, slightly steeper dips of these contacts in hanging wall (relative to their dips in the footwall) suggest slight folding has further deformed the units. Secondary fault splays with <5 cm of vertical separation are evident at meter 4.5 of the west wall and meter 12.5 of the east wall of Trench 5(Figure 14; Plate 1). All faults can be traced into the upper, massive part of Unit 300 where they can no longer be distinguished. The upper content of Unit 300 is nowhere cut by faulting and is buried sequentially by sand layers that comprise the basal section of Unit 400. The top of Unit 300 and base of Unit 400 therefore defines slight angular unconformity (U4).

Figure 13 and 14 show two unconformities, U3 and U4. The youngest of these, U4 is associated with a faulting event that cuts Unit 100-300. Subsequent burial by Units 400 and younger clearly show a slight angular unconformity at the base of Unit 400 (Figure 14 and 15; Plate 1). Another slight angular unconformity is present at the base of of Unit 200 (U3). Unlike U4 unconformity U3 is not associated with any faulting. Its origin is therefore equivocal.

Fissure-like fractures are present at the level of the top of Unit 400(Figure 16). However, careful inspection shows that these features are filled with seeds and twigs and have irregular shapes that are more consistent with large krotovina rather than fissures. In addition, no deformation related structure or stratigraphic features is associated with the top of Unit 400. The features shown in Figure 16 are therefore not considered to be earthquake related.

Figure 12. Fault zone exposed in east wall of Trench 5. White arrows point to two thrust splays cutting Units 100 and 200 at the base of the east wall of Trench 5. Splay at the left arrow can be followed to where it reaches the right edge of the photo (into sunlight) about 1/3 of the way down from the top of the photo. The splay at the right arrow can be followed to the right edge of the photo, mid-way along the right edge.

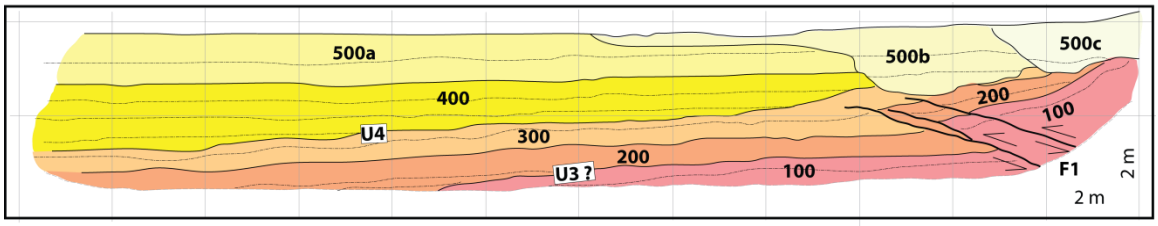

Figure 13. Simplified log of west wall T5. Perspective view is toward the west (left and right end of log is south and north, respectively). Thrust zone in Trench 5 dips 25°-30° N. Two unconformities can be recognized. The uppermost unconformity, U4, records the most recent rupture with strata above the unconformity (Units 400-500) burying a scarp cored(?) with thrusts that terminate at its base. Clear fault relations have not been recognized with base of Unit 200. A channel sequence in Unit 500 has eroded the top portion of the scarp.

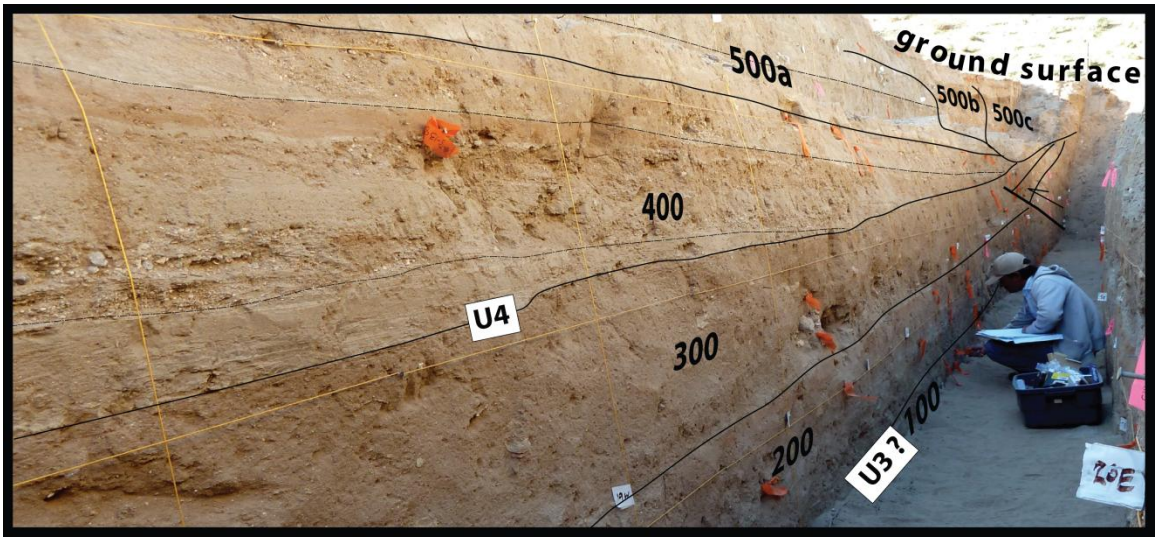

Figure 14. Oblique view of the west wall of T5. Units 100-500 consist of interbedded silty mud, fine to coarse sand, pebbly sand, and fine to coarse gravel. A distinct unconformity (U4) identifies the most recent earthquake (note thrust projected to base of U4 at back of trench). The thickening of Unit 200 away from the thrust might indicates the presence of an underlying unconformity, which is likely related to an earthquake that pre-dates the one related to U4.

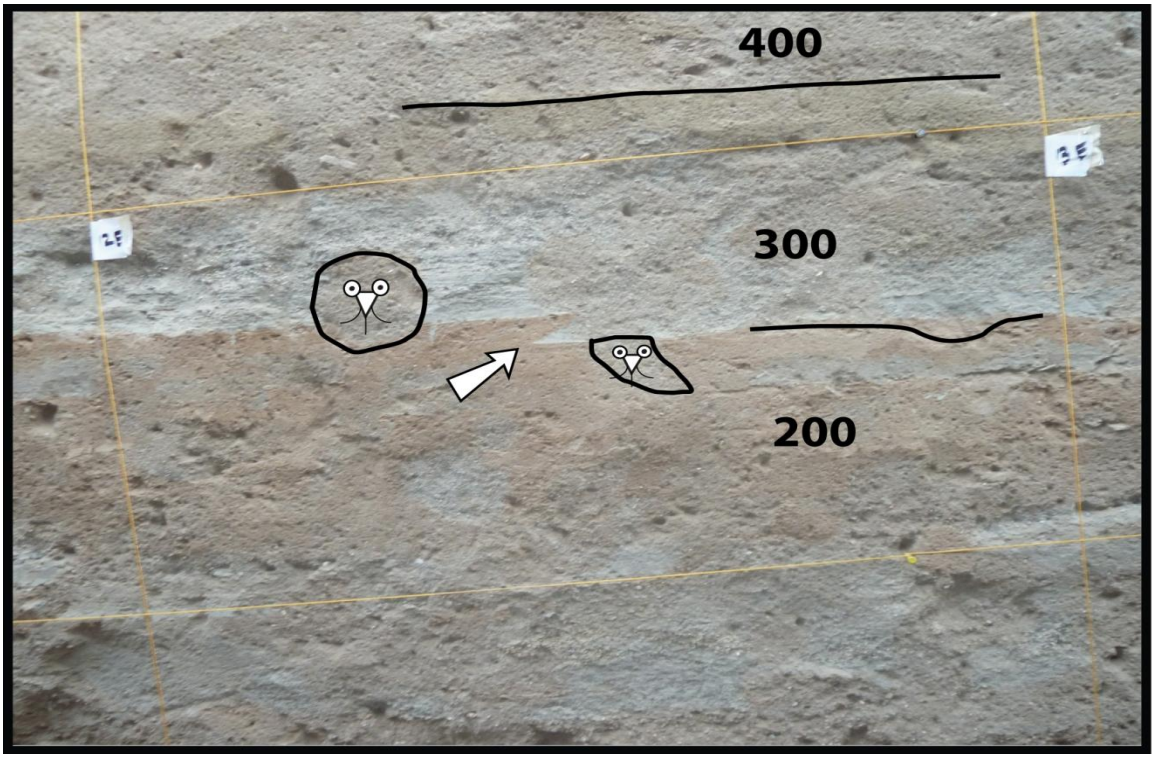

Figure 15. Secondary fault in east wall Trench 5 at m 12.5 E (east wall). See white arrow with ~5 cm of vertical separation. Burrows are outlined in black. Strong grid measures 0.5 m (vertical) × 1.0 m (horizontal).

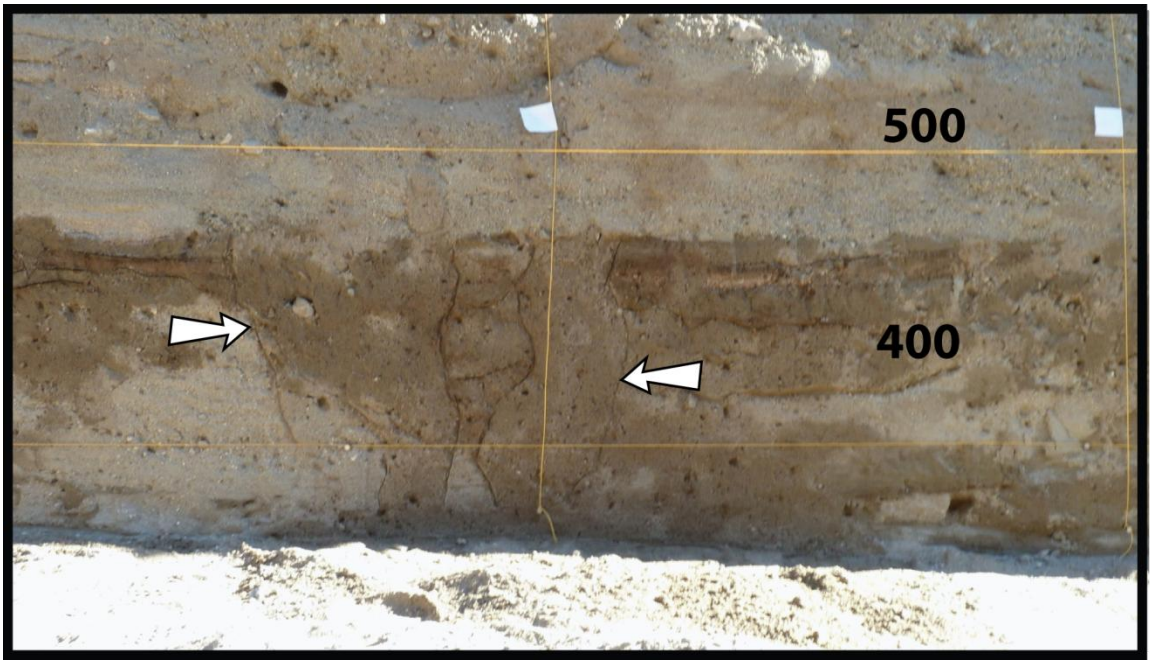

Figure 16. Bioturbated zones in the upper east wall of Trench 5 cut massive Unit 400. White arrows point to scraper marks, which highlight the sub-horizontal layering and the sub-vertical margins of cross-cutting burrow-like features (krotovina). Strong grid measures 0.5 m (vertical) × 1.0 m (horizontal).

RADIOCARBON AGE DATA

In order to determine the timing of most recent event, my field assistants and I collected detrital charcoal for radiocarbon dating from every unit of Trench 5 (Table 3). Table 5 summarize the ages obtained from samples analyzed. No samples were collected from Trench 6. Table 4 shows the result of ^{14}C analysis and calibration for this for this study. See Plate 1 for the exact sample positions.

Table 3. Detrital Charcoal Samples Collected in Trench 5

Stratigraphic unit	number of samples collected	number of samples analyzed
Unit 600	1 (west wall)	0
Unit 500a	11 (1 east wall; 10 west wall)	4 (L. Livermore)
Unit 400	32 (13 east wall; 19 west wall)	11 (2 Irvine; 9 L. Livermore)
Unit 300	14 (5 east wall; 9 west wall)	8 (L. Livermore; plus 1 duplicate)
Unit 200	37 (17 east wall; 20 west wall)	8 (1 Irvine; 7 L. Livermore)
Unit 100	10 (1 east wall; 9 west wall)	6 (1 Irvine; 5 L. Livermore)

All ^{14}C dates have been calibrated to calendar years BP (Table 4). Each calendar age provides a maximum limiting age for an earthquake event because the charcoal samples are all detrital pieces and thus there is an unknown amount of time required to incorporate the charcoal into sediment once formed. It is also possible that the charcoal may have been reworked from older deposits, increasing the time difference between charcoal age and depositional age. Therefore, at locations where more than one charcoal sample was collected from each unit, the youngest age from the sample set is considered the age of the unit, and older ages are not used to constrain unit age (Figure 17).

Thirteen of the 37 radiocarbon ages from detrital charcoal yield in-sequence ages, indicating that the strata in Units 100 to 500 were deposited between ~900 and 300 years ago (red probability distributions Figure 17). Twenty two of the samples are consider to be “too old”, either due to being reworked or having lengthy lag time before deposition

Table 4 Radio Carbon Age Data

CENTER FOR ACCELERATOR MASS SPECTROMETRY LAWRENCE LIVERMORE NATIONAL LABORATORY

UNIVERSITY OF CALIFORNIA IRVINE KECK LABORATORY

Submitter: Yule/Brown/SCEC

CAMS #	Sample Name	Stratigraphic units	Stratigraphic level	$d^{13}C$	fraction Modern	±	$D^{14}C$	±	^{14}C age	±	Calibrated Ages(BP) Oxcal v.4.1
151995	CAB11-T5-1	Unit 500	top	-25	0.9580	0.0032	-42.0	3.2	345	30	485-313
156042	CAB11-T5-46		middle	-25	0.9464	0.0033	-53.6	3.3	445	30	535-464
151996	CAB11-T5-50		middle	-25	0.8811	0.0089	-118.9	8.9	1020	90	1141-737
151997	CAB11-T5-42		bottom	-25	0.8859	0.0047	-114.1	4.7	975	45	965-785
156043	CAB11-T5-43	Unit 400	top	-25	0.9298	0.0032	-70.2	3.2	585	30	652-581
151998	CAB11-T5-55		top	-25	0.9057	0.0032	-94.3	3.2	795	30	765-672
156044	CAB11-T5-7		middle	-25	0.8999	0.0040	-100.1	4.0	845	40	802-681
156045	CAB11-T5-33		middle	-25	0.9014	0.0038	-98.6	3.8	835	35	797-681
156046	CAB11-T5-11		middle	-25	0.9063	0.0035	-93.7	3.5	790	35	770-670
151999	CAB11-T5-49		middle	-25	0.0000	0.0062	-1004.1	6.2	>35225		40936-40073*
152000	CAB11-T5-23		middle	-25	0.8965	0.0032	-103.5	3.2	875	30	834-726
152001	CAB11-T5-14		bottom	-25	0.9207	0.0034	-79.3	3.4	665	35	677-625

1) $d^{13}C$ values are the assumed values according to Stuiver and Polach (Radiocarbon, v. 19, p.355, 1977) when given without decimal places. Values measured for the material itself are given with a single decimal place.

2) The quoted age is in radiocarbon years using the Libby half life of 5568 years and following the conventions of Stuiver and Polach (ibid.).

3) Radiocarbon concentration is given as fraction Modern, $D^{14}C$, and conventional radiocarbon age.

4) Sample preparation backgrounds have been subtracted, based on measurements of samples of ^{14}C-free charcoal. Backgrounds were scaled relative to sample size.

5) Sample CAB11-T5-32 yielded less than 20µg of carbon and a result is not reported.

6) Gray shaded ages are not in-sequence

* Not shown on plot because too old

Table 4 (continued) Radiocarbon Age Data

CENTER FOR ACCELERATOR MASS SPECTROMETRY LAWRENCE LIVERMORE NATIONAL LABORATORY

UNIVERSITY OF CALIFORNIA IRVINE KECK LABORATORY

Submitter: Yule/Brown/SCEC

CAMS #	Sample Name	Stratigraphic units	Stratigraphic level	$d^{13}C$	fraction Modern	±	$D^{14}C$	±	^{14}C age	±	Calibrated Ages(BP) Oxcal v.4.1
152002	CAB11-T5-12	Unit 400	bottom	-25	0.9044	0.0040	-95.6	4.0	805	40	788-672
90340	CAB11-T5-9		bottom		0.8940	0.8940	-106.0	1.7	900	20	833-741
90341	CAB11-T5-34		bottom		0.9290	0.9290	-71.0	1.7	590	15	641-589
152003	CAB11-T5-117	Unit 300	top	-25	0.9020	0.0032	-98.0	3.2	830	30	791-686
156048	CAB11-T5-151		middle	-25	0.8924	0.0031	-107.6	3.1	915	30	920-764
156049	CAB11-T5-107		middle	-25	0.8781	0.0031	-121.9	3.1	1045	30	1005-921
152004	CAB11-T5-124		middle	-25	0.8668	0.0034	-133.2	3.4	1150	35	1150-974
152017	CAB11-T5-124 dup		middle	-25	0.8712	0.0031	-128.8	3.1	1105	30	1066-937
152005	CAB11-T5-116		middle	-25	0.8597	0.0035	-140.3	3.5	1215	35	1189-1059
152006	CAB11-T5-106		middle	-25	0.8643	0.0032	-135.7	3.2	1170	30	1175-1049
152019	CAB11-T5-106 dup		middle	-25	0.8648	0.0029	-135.2	2.9	1165	30	1174-1048
152007	CAB11-T5-101		bottom	-25	0.8584	0.0031	-141.6	3.1	1225	30	1188-1065

1) $d^{13}C$ values are the assumed values according to Stuiver and Polach (Radiocarbon, v. 19, p.355, 1977) when given without decimal places. Values measured for the material itself are given with a single decimal place.

2) The quoted age is in radiocarbon years using the Libby half life of 5568 years and following the conventions of Stuiver and Polach (ibid.).

3) Radiocarbon concentration is given as fraction Modern, $D^{14}C$, and conventional radiocarbon age.

4) Sample preparation backgrounds have been subtracted, based on measurements of samples of ^{14}C-free charcoal. Backgrounds were scaled relative to sample size.

5) Sample CAB11-T5-32 yielded less than 20µg of carbon and a result is not reported.

6) Gray shaded ages are not in-sequence

Table 4 (continued) Radiocarbon Age Data

CENTER FOR ACCELERATOR MASS SPECTROMETRY LAWRENCE LIVERMORE NATIONAL LABORATORY

UNIVERSITY OF CALIFORNIA IRVINE KECK LABORATORY

Submitter: Yule/Brown/SCEC

CAMS #	Sample Name	Stratigraphic units	Stratigraphic level	$d^{13}C$	fraction Modern	±	$D^{14}C$	±	^{14}C age	±	Calibrated Ages(BP) Oxcal v.4.1
152008	CAB11-T5-17	Unit 200	top	-25	0.8972	0.0189	-102.8	18.9	870	170	1142-543
156050	CAB11-T5-100		middle	-25	0.7621	0.0027	-237.9	2.7	2185	30	2314-2120
156051	CAB11-T5-16		middle	-25	0.8686	0.0035	-131.4	3.5	1130	35	1143-960
90339	CAB11-T5-108 .090mgC		middle		0.8460	0.0019	-154.0	1.9	1345	20	1304-1261
152009	CAB11-T5-6		middle	-25	0.8721	0.0031	-127.9	3.1	1100	30	1063-937
152010	CAB11-T5-111		bottom	-25	0.8668	0.0061	-133.2	6.1	1150	60	1183-935
152011	CAB11-T5-128		bottom	-25	0.8730	0.0031	-127.0	3.1	1090	30	1058-936
156052	CAB11-T5-119	Unit 100	top	-25	0.8702	0.0041	-129.8	4.1	1115	40	1093-934
156053	CAB-T5-149		middle	-25	0.8511	0.0036	-148.9	3.6	1295	35	1296-1171
90338	CAB11-T5-141 .19mgC		middle		0.8831	0.0017	-116.9	1.7	1000	20	962-905
152012	CAB11-T5-150		middle	-25	0.8109	0.0035	-189.1	3.5	1685	35	1695-1525
152013	CAB11-T5-21		bottom	-25	0.7865	0.0055	-213.5	5.5	1930	60	1999-1717
152014	CAB11-T5-28		bottom	-25	0.8640	0.0039	-136.0	3.9	1175	40	1180-978

1) $d^{13}C$ values are the assumed values according to Stuiver and Polach (Radiocarbon, v. 19, p.355, 1977) when given without decimal places. Values measured for the material itself are given with a single decimal place.

2) The quoted age is in radiocarbon years using the Libby half life of 5568 years and following the conventions of Stuiver and Polach (ibid.).

3) Radiocarbon concentration is given as fraction Modern, $D^{14}C$, and conventional radiocarbon age.

4) Sample preparation backgrounds have been subtracted, based on measurements of samples of ^{14}C-free charcoal. Backgrounds were scaled relative to sample size.

5) Sample CAB11-T5-32 yielded less than 20µg of carbon and a result is not reported.

6) Gray shaded ages are not in-sequence

(gray probability distributions Figure 17). The two samples with blue probability distributions (Figure 17) may represent young charcoal that has been somehow bioturbated into strata with slightly older ages or in-situ charcoal that is slightly younger that majority of other in-sequence charcoal samples.

The calendar age of T5-34 closely overlaps the calendar ages of T5-14 and T5-43. These three samples, in addition to the calendar age of T5-117 constrain the age of U4 to 581-791 years BP (Figure 17). Using sample T5-141 constrains the age U3 constrains to between ~934-1093 years BP, our preferred age (Figure 17). If sample T5-141 is not included with in-sequence ages then U3 is between ~905-1183 years BP. More charcoal ages from Units 100 and 200 are needed to either rule out or confirm sample T5-141 as valid age. The ranges of ^{14}C calendar ages in both Units 100 and 200 are similar; hence, no distinction in age be can be made between the two oldest units.

Table 5. Summary of ^{14}C Calendar Ages (yrs. BP) from Table 5. Number of analyses shown in parentheses.

Stratigraphic unit	range of all ages	range of in-sequence ages	youngest in-sequence age
Unit 500a	313-1141 (4)	313-535 (2)	313-485
Unit 400	581-834 (11)	581-677 (3)	581-652
Unit 300	686-1189 (8)	686-1005 (3)	686-791
Unit 200	543-2314	935-1183 (4)	935-1183
Unit 100	934-1999	934-1180 (2)	934-1093

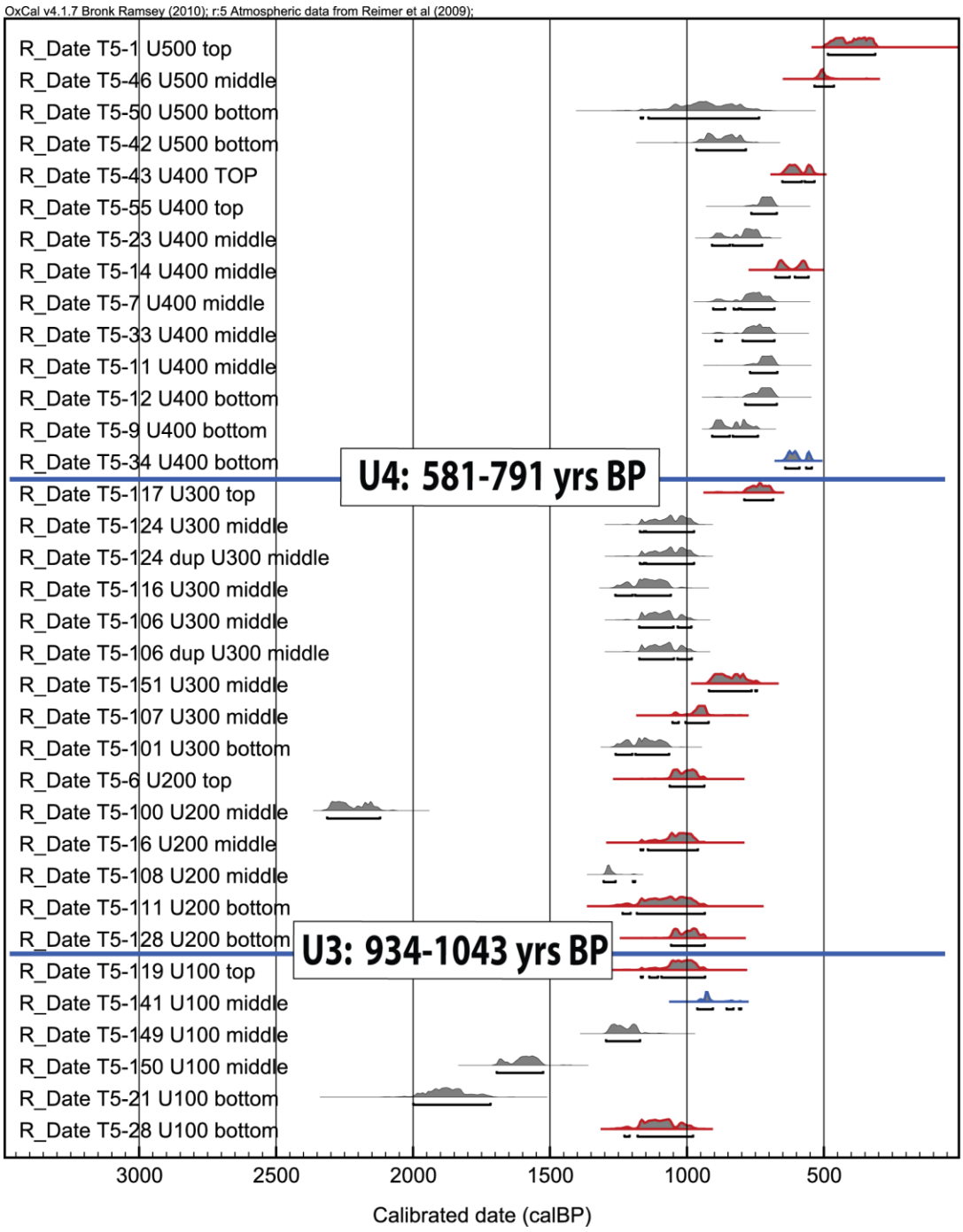

Figure 17. Stratigraphic position versus calibrated calendar ages (BP) of charcoal samples collected from the Trench 5. Out-of-sequence ages are shown in gray, in-sequence ages are shown red, and in blue unusually (?) young charcoal. The ages are plotted as probability distribution functions, with the peaks indicating the most likely calendar age. Blue horizontal lines with capital 'U' are unconformities thought to record earthquake rupture; the age of each unconformity is shown as deformed by the bounds of calendar ages from samples above and below.

DISCUSSION

Conceptual model of deformation caused by Event I

Figure 18A-G shows a schematic representation of events that produced the relations observed in Trench 5. Figure 18 A shows the pre-faulting stratigraphy consisting of Units 100, 200, 300 and the future location of the fault rupture. Strata across both sides of the fault rupture have the same thickness and are laterally continuous. Figure 18 B shows rupture during Event 1 and offset of Units 100, 200, and 300. Followed by erosion of scarp in the hanging wall and deposition of a small colluvial wedge in the footwall. Figure 18C shows deposition of Unit 400 across the scarp and Unit 300 and formation of angular unconformity U4, followed by deposition of Unit 500. Following deposition of Unit 500a, a SE flowing stream cuts small channels into Unit 500a on the hanging wall, subsequently filled by channel deposits of Units 500 b and c (Figure 18D). The final event is the deposition of Unit 600, which forms the modern surface of the fan in the area of Trench 5 (Plate 1).

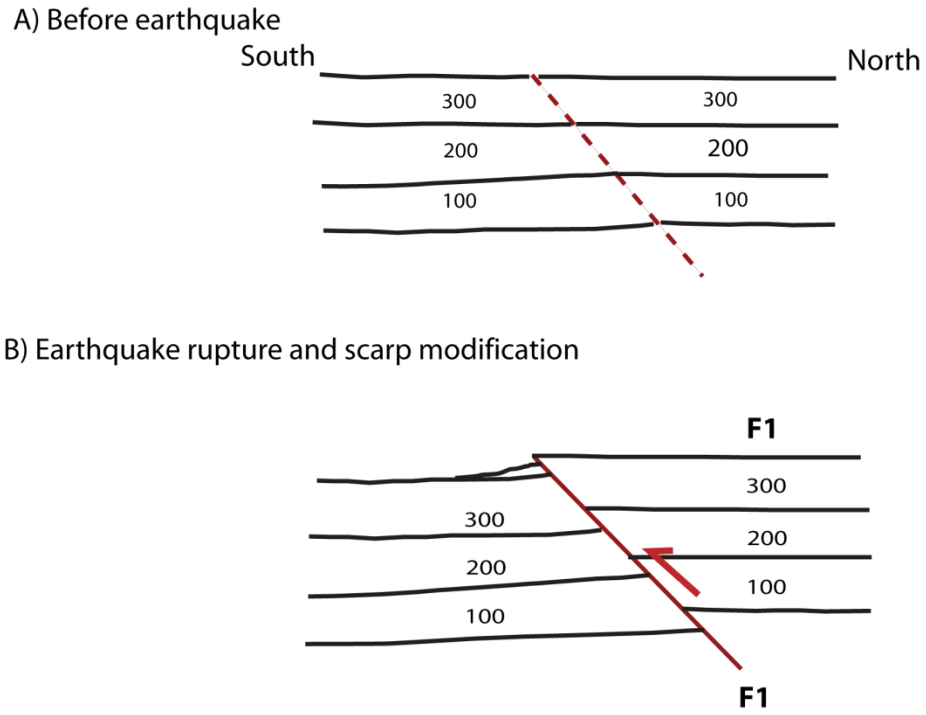

Figure 18. Conceptual model sequence of events.

Event record at Cabazon Trench 5

Trenching at the Cabazon site for this study identified only one distinct paleo-earthquake, designated as Event I, from the presence of a fault zone that cuts through Units 100, 200 and 300 in both walls of Trench 5. The splays of the fault zone do not reach Unit 400, which buries the scarp formed by the fault. These relations define an angular unconformity between Units 300 and 400. Event I therefore occurred prior to the deposition of Unit 400.

A possible earlier event is suggested by the onlap relation of the basal Unit 200 layers and slight thickening of Unit 200 away from the fault (Plate 1, Figure 13), but the depth of the trench is not sufficient to determine a clear picture of how U3 formed. If the onlap and thickening is fault related, the base of Unit 200 (U3) may record the penultimate rupture event in this area. However, it is also possible that this unconformity (U3) is not a deformation related but a stratigraphic unconformity between interfingering lenses of alluvium (perhaps interfingering layers of the Lion and Millard Canyon alluvial fans).

The ages of the unconformities in Trench 5 (U3 and U4) can be constrained by the available calibrated calendar year ages of radiocarbon samples. Assuming that U4 records the most recent earthquake, this event is constrained by samples T5-43 and T5-117 (Figure 17) to have happened 581 to 791 years BP. If U3 records a penultimate event it constrained by samples T5-119 and T5-111 to have happened to 934 to 1183 years BP. Alternatively U3 can be constrained by samples T5-141 and T5-111 to have occurred 905 to 1183 years BP. Future work that involves deepening Trench 5 can test whether U3 is a deformation or stratigraphy related feature.

Other active fault studies in San Gorgonio Pass

Millard Canyon contains two prominent fault scarps, a northern and southern scarp respectively. The northern splay of fault expressed by 2.5 ± 0.7 m and 5.0 ± 0.7 m scarps in alluvial terraces constrained to be ~1200 and ~2500 yrs old, respectively (Yule et al., 2011). Recent studies in this area (McBurnett, 2011) constrain four earthquakes at this site since ~2500 years BP and two earthquakes since ~1300 years BP. The southern Millard Canyon scarp varies in hight, reaching a maximum height of 12.5 m and the minimum level of 1.5 m (Yule and Sieh, 2003). The highest level of southern scarp reflects multiple earthquakes and lowest level probably the most recent event. The lowest level is a terrace that inset into the ~1200 years old terrace, and the 2.5 m scarp of northern Millard Canyon therefore must be <1200 years old.

A 1997 study at the Cabazon site (Yule et al., 1997) exposed 20 m-wide fault zone extending south from base of the hill. This study documented three main ruptures in four trenches and four unconformities (U1 to U4). U4 is probably the same as U4 as defined in Trench 5 (this study). Radiocarbon ages constrain the age of U4 at Trench 1-4 between 500 to 710 years BP, in overlap with the age given in this study for U4 in Trench 5 (Figure 13 and Figure 17). No ages are reported for U1 to U3 in Yule's 1997 study.

Summary of data from San Gorgonio Pass studies

A summary of the paleoseismic data from this and previous studies is shown in Table 6. Timing of the most recent earthquakes from the Millard Canyon sites are not well constrained. The Cabazon sites are consistent in constraining an event to the 13th - 14th century. The most recent event at all four sites generated >1.5 m scarp, roughly 5 m

of slip resolved N45°W-S45°E on 30°-dipping oblique-slip thrust faults. Large slip suggests rupture during a single event (e.g. Biasi et al., 2009).

Table 6. Summary of paleoseismic data from San Gorgonio Pass

Site	Age of most recent earthquake rupture
Millard Canyon North	<1200 years BP (two events)
Millard Canyon South	<1200 years BP
Cabazon Trench 1-4 (Yule et al., 1997)	500-710 years BP
Cabazon Trench 5 (This study)	581-791 years BP

Possible correlation of San Andreas ruptures through San Gorgonio pass

Work at other paleosismic sites on San Andreas fault to the northwest and southeast of San Gorgonio Pass give different recurrence intervals. For example, the Mojave section of the fault yield average recurrence of ~100 years (e.g. Weldon et al., 2004). The Coachella Valley region appears to have earthquakes every ~200-250 years (e.g. Philibosian et al., 2011).

But in San Gorgonio Pass recurrence appears to the longest, 650 years. Another illustration of this difference can be seen in Figure 19 where the Wrightwood site has experienced 10 events, the Coachella Valley site 7 events, and the Cabazon site 1 and possibly (?) 2 events in the last 1300 years. Furthermore, neither the 1812 nor the late 17th century ruptures are evidenced at Cabazon. These data support a model where the San Andreas fault ruptures more frequently with "Pass-as-a barrier" earthquakes and less frequently with through-going San Gorgonio Pass events.

The latter type of earthquake is indicated by the gray bars on Figure 19. The mid-14th century correlation on Figure 19 may record a possible 'super' earthquake

correlations for the southern San Andreas fault an event may involve rupture the Coachella Valley, San Bernardino, and Mojave sections (and beyond?) of the fault. The most recent possible through-going event at San Gorgonio Pass can be defined by selecting the following events from other paleoseismic sites whose event timing overlap. From NW and SE, this possible super earthquake includes Event T at Pallett Creek, Event 5 at Pitman Canyon, Event R at Plunge Creek, Event 5 at Burro Flats, Event 1 at Cabazon, Event 3 at Indio, and Event 4 at Coachella, and also Millard Canyon, McBurnett, 2011 (Figure 19).

Is this through-going correlation a super earthquake on the southern San Andreas fault, rare but very large event? If so it may be worthwhile to revisit event evidence at the various paleoseismic sites to explore the possible super earthquake (as defined above) generated usually large displacement. Events 1-4 at Burro Flats site produced only folding, where deformation associated with Event 5 at Burro Flats caused multiple ruptures and fissures to form in addition to folding. Event 5 at Burro Flats does appear to be larger event than the later events do not appear to have ruptured the San Gorgonio Pass fault zone.

Implication for San Andreas fault behavior.

The finding from my work in Trench 5 agrees and strengthens findings from previous studies of active thrust faults in San Gorgonio Pass (Yule et al., 1997, Yule et al., 2011, McBurnett, 2011). These data suggest that ruptures occur here 2-4 times less frequently on strike-slip strands of the San Andreas fault to the NW and SE. The data also permit a correlation in time for through-going event ~650 years ago that may have simultaneously ruptured the Coachella Valley, San Gorgonio Pass, San Bernardino, and Mojave segments of the fault. If correct these data support a model where the San Gorgonio Pass acts both arrests earthquake ruptures, as it has apparently done since the late middle ages and allows through-going ruptures, as it appears to have last done in the 14th century.

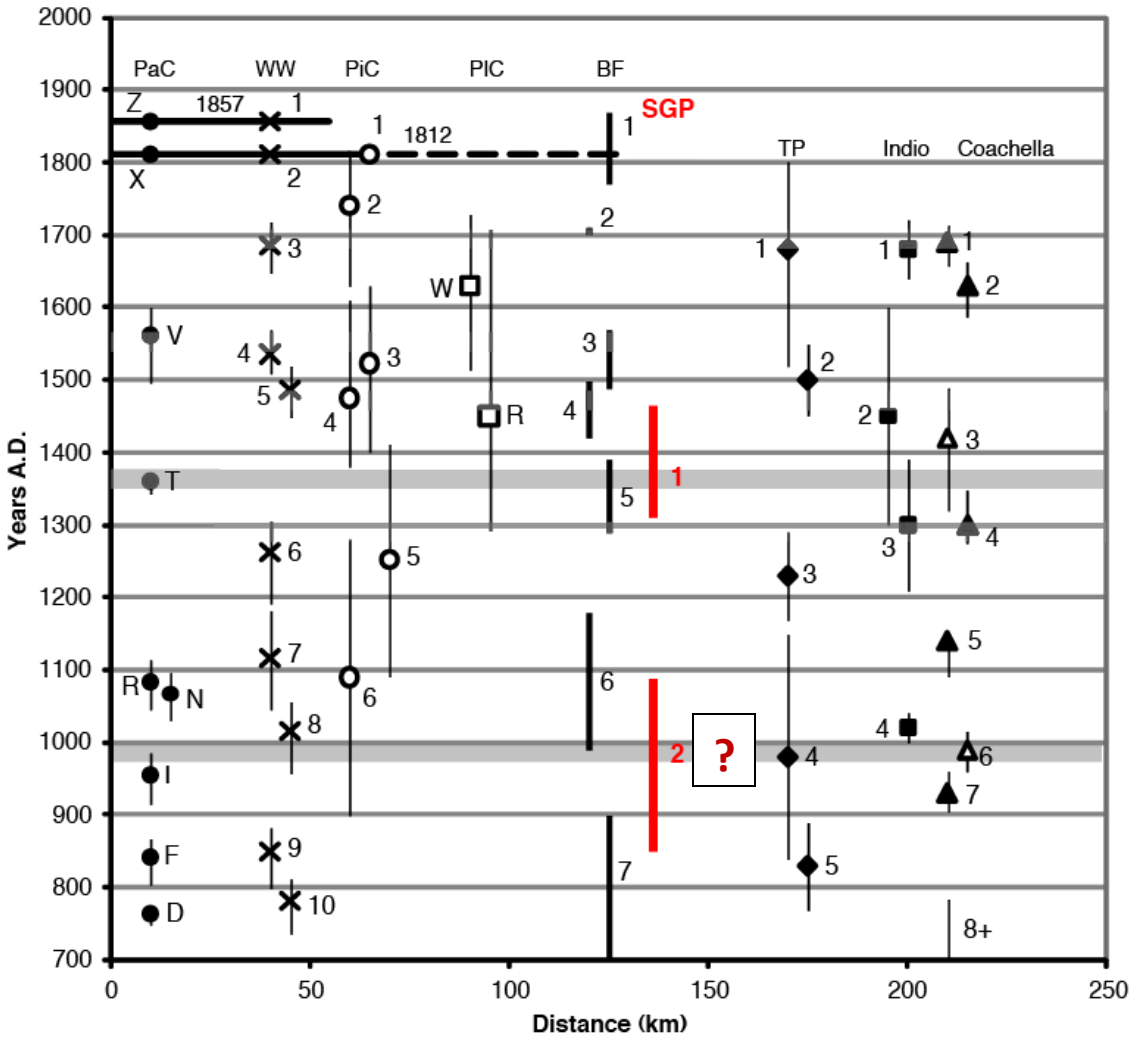

Figure 19. Modified *Figure 17* of *Philibosian et al., 2011*. Earthquake chronologies from paleoseismic sites on the San Andreas fault with new data from the Cabazon site in San Gorgonio Pass shown as red vertical bars. Black horizontal bars show the rupture extent of the 1857 and 1812 earthquakes. Gray horizontal bars show possible correlations between sites and possible 'super' earthquakes correlations for the southern San Andreas fault, those that may rupture the Coachella Valley, San Bernardino, and Mojave sections (and beyond?) of the fault. Black horizontal bars show rupture extents of the historical 1857 and 1812 earthquakes. Site abbreviations: PaC: Pallett Creek, WW: Wrightwood, PiC: Pitman Canyon, PlC: Plunge Creek, BF: Burro Flats, SGP: San Gorgonio Pass, TP: Thousand Palms.

Future Work

Results of this study support the model of Yule and Sieh (2003) and Carena et al. (2004) that proposes that the system of numerous strike slip and reverse faults that form the fault zone of San Gorgonio Pass that can rupture in a complex way to allow through-going rupture, such as that proposed by the 2008 ShakeOut scenario (Jones et al., 2008). However, this study also shows that through-going rupture events are infrequent. Hence, results support both the "Pass-as-barrier" and "through-going" rupture models.

More trench studies at the Cabazon site are necessary to link the chronologies of rupture events in San Gorgonio Pass with those on adjacent north and south segments of San Andreas fault. Trench 5 exposes a single fault zone, but the rest of the fault zone identified by previous studies was not excavated because I was unable to gain permission to extend Trench 5 and Trench 6 across the roads. For future work we purpose a mega-trench at Cabazon, where a long event (~3000 year) record can be potentially be established across the San Gorgonio Pass.

CONCLUSIONS

1. The stratigraphic, structural, and radiocarbon analyses of sedimentary units of Trench 5 constrain the most recent earthquake on the San Gorgonio Pass fault zone at~600-800 yrs BP. This event can be correlated with earlier studies at Cabazon (Yule et al., 1997) and Millard Canyon sites (Mcburnett, 2011).

2. Neither the 1812 nor the 1680 San Andreas fault events occurred at Cabazon, suggesting that possible through-going San Andreas fault ruptures, if they occur, happen relatively infrequently.

3. Trench 5, located where two large fans merge, receives relatively fine-grained, charcoal rich detritus making this a quality paleoseismic site. The excellent stratigraphy discovered here makes this an intriguing location for future work, perhaps a ‘mega trench’, where a long event record can potentially be possibly established across the San Gorgonio Pass.

4. These findings have major impact on the understanding of enigmatic San Gorgonio Pass. We constrained the age of most recent earthquake, and we did not observe with certainty another rupture event in Trench 5. Unconformity surface U3 might represent another rupture event. However, the incomplete exposure and the poorly constrained age are insufficient for a reliable recurrence interval and slip rate to be determined.

REFERENCES

Akciz, Sinan O., Grant Loudwig, Lisa, Arrowsmith, J Ramon, 2009. Revised dates of large earthquakes along the Carrizo section of the San Andreas Fault, California, since A.D. 1310±30. Journal of Geophysical Research, v. 114, B01313.

Allen, C.R., 1957, San Andreas fault zone in the San Gorgonio Pass, southern California: Geological Society of America Bulletin, v. 68, p. 315–350.

Becker, Thorsten W., Hardebeck, Heanne L., Anderson, Greg, 2005. Constraints on fault slip rates of the southern California plate boundary from GPS velocity and stress inversions, Geophys. J. Int., 160, pp. 634-650.

Behr, W.M., Rood, D.H., Fletcher, K.E., Guzman, N., Finkel, R., Hanks, T.C., Hudnut, K.W., Kendrick, K.J., Platt, J.P., Sharp, W.D., Weldon, R.J., Yule, J.D., Uncertainties in slip-rate estimates for the Mission Creek strand of the southern San Andreas Fault at Biskra Palms Oasis, southern California, Geological Society of America Bulletin, v. 122; no. 9-10; p. 1360-1377.

Bennett, R. A., W. Rodi, and R. E. Reilinger, Global Positioning System constraints on fault slip rates in southern California and northern Baja, Mexico, Journal of Geophysical Research, v. 101, B10. 21, 943-21, 960.

Biasi, G. P., R. J. Weldon, T. E. Fumal, and G. G. Seitz (2002). Paleoseismic event dating and the conditional probability of large earthquakes on the southern San Andreas fault, California, Bull. Seismol. Soc. Am. 92, 2761–2781.

Carena, S., Suppe, J., and Kao, H., 2004, Lack of continuity of the San Andreas fault in southern California: Threedimensional fault models and earthquake scenarios: Journal of Geophysical Research, v. 109, no. B4, paper B04313.

Cook, M. L., Dair, L., Simulating the recent evolution of the southern big bend of the San Andreas fault, Southren California. Journal of Geophysical Research, v. 116, B04405.

Fumal, T. E., Weldon II, R. J., Biasi, G P., Dawson, T. E., Seitz, G. G., Frost, W.T., Schwartz, D. P., 2002. Evidnce for large earthquakes on San Andears fault at Wrightwood, California, paleoseismic site: A.D. 500 to present. Bulletin of the Seismological Society of America, Vol. 92, No. 7, pp. 2726-2760.

Harden, J.W., And Matti, J.C., Holocene and late Pleistocene slip rates on the San Andreas fault in Yucaipa, California, using displaced alluvial-fan deposits and soil chronology. Geological Society of America Bulletin, v 101, p. 1107-1117.

Hauksson, E., 2000, Crustal structure and seismicity distribution adjacent to the Pacifi c and North America plate boundary in southern California: Journal of Geophysical Research, v. 105, no. B6, p. 13,875–13,903.

Jones, L., Hutton, Given D., and Allen C., 1986, The North Palm Springs, California, earthquake sequence of July 1986: Seismological Society America Bulletin, v. 76, no. 6, p. 1830-1837.

Jones L.M., Bernknopf, R., Cox, D., Goltz, J., Hudnut, K., Mileti, D., Perry, S., Ponti, D., Porter, K., Reichle, M., Seligson, H., Shoaf, K., Treiman, J., and Wein, A., 2008, The ShakeOut Scenario: U.S.Geological Survey Open File Report 2008-1150, California Geological Survey Preliminary Report 25, version 1.0, 312 p.

Keller, E. A., Bonkowski, M. S., Korsch, R. J., Shlemon, R. J., 1982. Tectonic geomorphology of the San Andreas fault zone in the southern Indio Hills, Coachella Valley, California. Geological Society of America Bulletin, Vol. 93, pp. 45-56.

Langenheim, V.E., Jachens, R.C., Matti, J.C., Hauksson, E., Morton, D.M., and Christensen, A., 2005, Geophysical evidence for wedging in the San Gorgonio Pass structural knot, southern San Andreas fault zone, southern California: Geological Socieity of America Bulletin, v. 117; no. 11/12, p. 1554–1572.

Magistrale, H., and Sanders, C., 1996, Evidence from precise earthquake hypocenters for segmentation ofthe San Andreas fault in San Gorgonio Pass: Journal of Geophysical Research, v. 101, p. 3031–3041.

Matti, J.C., and Morton, D.M., 1993, Paleogeographic evolution of the San Andreas fault in southern California: A reconstruction based on a new cross-fault correlation, in Powell, R.E.,Weldon, R.E., II, and Matti, J.C., eds., The San Andreas fault system: Displacement, palinspastic reconstruction, and geologic evolution: Geological Society of America Memoir 178, p.107–159.

Matti, J.C., Morton, D.M., and Cox, B.F., 1985, Distribution and geologic relations of fault systems in the vicinity of the central Transverse Ranges, southern California: U.S. Geological Survey Open-File Report 85-365, 23 p.

Matti, J., Morton, D., Cox, B., 1992, The San Andreas fault system in the vicinity of the central Transverse Ranges province, southern California, U.S. Geological Survey Open File Report 92-354, 40 pp.

McBurnett, P., 2011, Paleoseimicity of the San Gorgonio Pass Fault Zone at the Millard Canyon: Testing the likelihood of a through-going San Andreas rupture [M.S. thesis]: California State University Northridge.

McGill, S., Weldon, R.J., II, Kendrick, K., and Owen, L., 2006, Late Pleistocene slip rate of theSan Bernardino strand of the San Andreas fault in Highland: Possible confirmation of the low rate suggested by geodetic data: Seismological Research Letters, v. 77, no. 2, p. 279.

Orozco, A.A., 2004, Offset of a mid-Holocene alluvial fan near Banning, CA; constraints on the slip rate of the San Bernardino strand of the San Andreas fault [M.S. thesis]: California State University Northridge.

Philibosian, B., Fumal, T., and Weldon, R., 2011, San Andreas Fault Earthquake Chronology and Lake Cahuilla History at Coachella, California, Bulletin of the Seismological Society of America, Vol. 101, No. 1, pp. 13–38, February 2011.

Powell, R. E. and Weldon, R.J. 1992, Evolution of the San Andreas fault, Annu. Rev. Earth Planet. Sci. v. 20, 431-468.

Rasmussen, G., Reeder, W., 1986. What happens to the real San Andreas fault at Cotton wood canyon, San Gorgonio Pass, California?. Geology Around the Margins of the Eastern San Bernardino Mountains, Inland Geological Society, Redlands, California, pp.157-162.

Scharer, K.M., Biasi, G. P., Weldon, R. J. II, Fumal, T. E., 2010. Quasi-periodic recurrence of large earthquakes on the southern San Andreas fault, Geology. 38, 555-558.

Scharer, K., R. Weldon, T. Fumal, and G. Biasi (2007). Paleo-earthquakes on the southern San Andreasfault, Wrightwood, California, 3000 to 1500 B.C., Bull. Seismol. Soc. Am. 97, 1054–1093.

Seeber, L., and Armbruster, J.G., 1995, The San Andreas fault system through the Transverse Ranges as illuminated by earthquakes: Journal of Geophysical Research, v. 100, no. B5, p.8285–8310.

Shifflett, H., M.G.Gray, R. Grannell, and B. L. Ingram (2002), New evidence on the slip rate, renewal time, and late Holocene surface displacement, southern most San Andreas fault, Mecca Hills, Bulletin of the Seismological Society of America, Vol. 92, No. 7, pp. 2861-2877, October.

Sykes, L.R., and Seeber, L., 1985, Great earthquakes and great asperities, San Andreas fault, southern California: Geology, v. 13, p. 835–838.

Stone, Elizabeth, Grant, Lisa B., Arrowsmith, J Ramon, 2002. Recent Rupture History of the San Andraes Fault Sotheast of Cholame in the Northren Carrizo Plain, Californai. Bulletin of the Seismological Society of America, Vol. 92, No. 3, pp. 983-997, April.

Spotila, J., Farley, K., Sieh, K., 1998. Uplift and erosion of the San Bernardino Mountains associated transpression along the San Andreas fault, California, as constrained by radiogenic helium thermochronology. Tectonics, Vol. 17, pp360-378.

Toke, Nathan A., Arrowsmith, J. Ramon, Rymer, Michael J., Landgraf, Angela, Haddad, David E., Bush, Melanie, Coyan, Joshua, Hannah, Alexander, 2011. Late Holocene slip rate of the San Andreas fault and its accommodation by creep and moderate-magnitude earthquakes at Parkfield, California, Geological Society of America, Vol. 39, N.3, pp. 243-246, March.

Van der Woerd, J., Klinger, Y., Sieh, K., Tapponnier, P., Ryerson, F.J., and Meriaux, A.S., Long-term slip rate of the southern San Andreas Fault from Be-10-Al-26 surface exposure dating of an offset alluvial fan: Journal of Geophysical research-Solid Earth, v.111, no.B4.

Weldon, R.J., II and Sieh, K. E., 1985, Holocene rate of slip and tentative recurrence interval for large earthquakes on the San Andreas fault, Cajon Pass, Southern California. Geological Society of America Bulletin, v 96, p. 793-812.

WGCEP (Working Group on California Earthquake probabilities) 2008. The Uniform California Earthquake Rupture Forecast, Vol. 2, USGS Open File Report 2007.

Young, Jeri J., Arrowsmith, J. Ramon, Colini, Laura, Grant, Lisa B., Gootee, Brian, 2002. Three-Dimnensional Excavation and Recent Rupture History along the Cholame Segment of the San Andreas Fault. Bulletin of the Seismological Society of America, Vol. 92, No. 7, pp. 2670-2688.

Yule, D., McBurnett, P., and Ramzan, S., 2011, Long Return Periods for Earthquakes in San Gorgonio Pass and Implications for Large Ruptures of the San Andreas Fault in Southern California, Abstract S21A-2141, Fall Meeting, AGU, San Francisco.

Yule, D., 2009. The enigmatic San Gorgonio Pass: Geological Society of America. V. 37, no. 2; p. 191–192.

Yule, D., and Sieh, K., 2001, The paleoseismic record ar Burro Flats: Evidence from a 300 year average recurrence for large earthquakes on the San Andreas fault in San Gorgonio Pass, sothren California. Paper presented at the 97th Annual Meeting, Geological Society of America Cordilleran Section, Pacific Section of American Association of Petroleum Geologist, Universal City, California.

Yule, D., and Sieh, K., 2003, Complexities of the San Andreas fault near San Gorgonio Pass: Implications for large earthquakes: Journal of Geophysical Research, v. 108, no. B11, ETG 9-1–9-23.

Yule D., Sieh, K., and Liu, J., 1997, Late Holocene Paleoseismicity and slip rate of the San Gorgonio Pass fault: Implications for through-going San Andreas rupture events, SCEC Annual Meeting Abstracts with Programs, Costa Mesa, CA, p. 95-96.

Appendix A

Hand excavated mini trench

We manually excavated 0.5 m deep and 6 m long trench in to the east wall of Trench 5. The purpose of this mini trench was to confirm the fault zone F1 in upper wall and also to examine the 3D view. We observed that fault zone expressed as two strands in the upper wall and disappear close to the bench (Figure 1.1). This small excavation confirmed the die out of fault tip in Unit 300. Another purpose of this mini trench was to confirm the connection between a long burrow and fault lineament at meter mark 5. The image sequence of the excavation (Figure A1.2 & A1.3 A-E) shows that the burrow disappears laterally and that unconformity surface U4 is laterally continuous in this section of the trench wall.

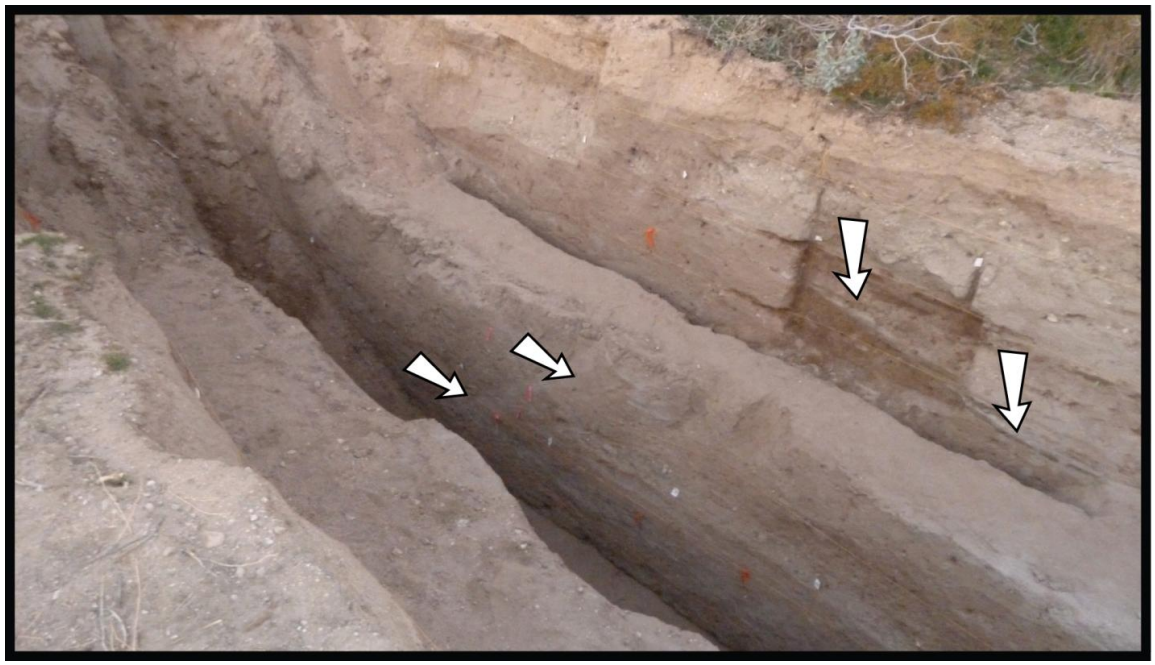

Figure A 1.1. Hand excavated mini trench cut into bench between lower and upper walls of east wall of Trench 5. Upper photo: Two parallel arrows at left point to thrust splays. Two vertical arrows point down locate U4 (unconformity). Lower photo: Simplified log of exposures. See Figure 24 for a detailed log of this exposure.

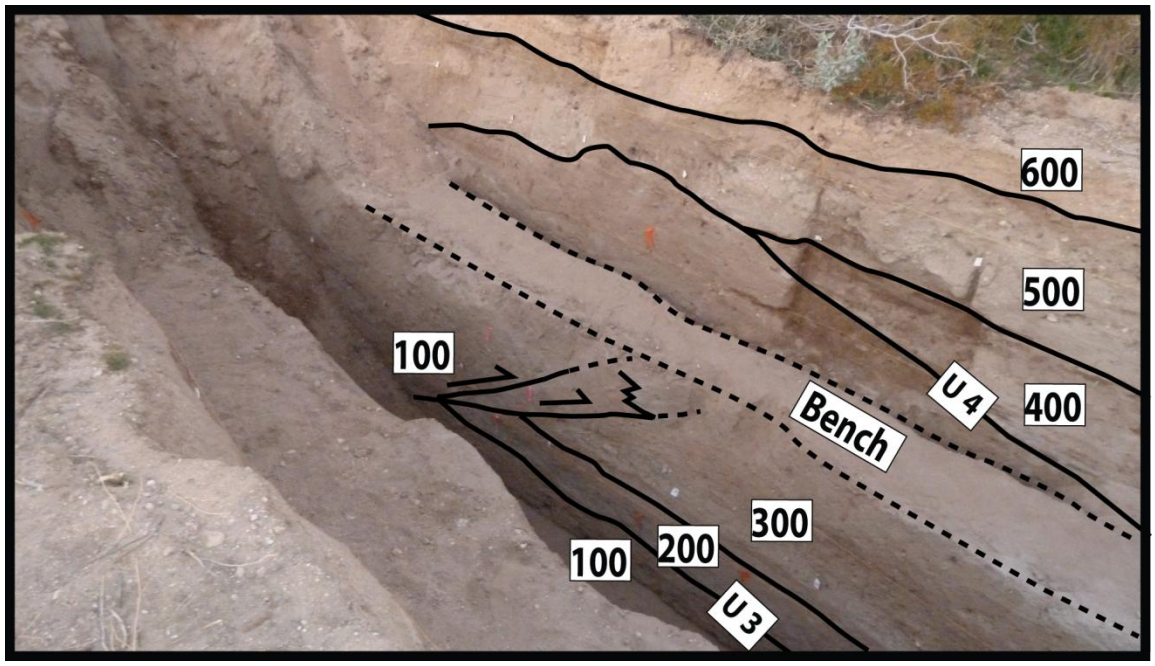

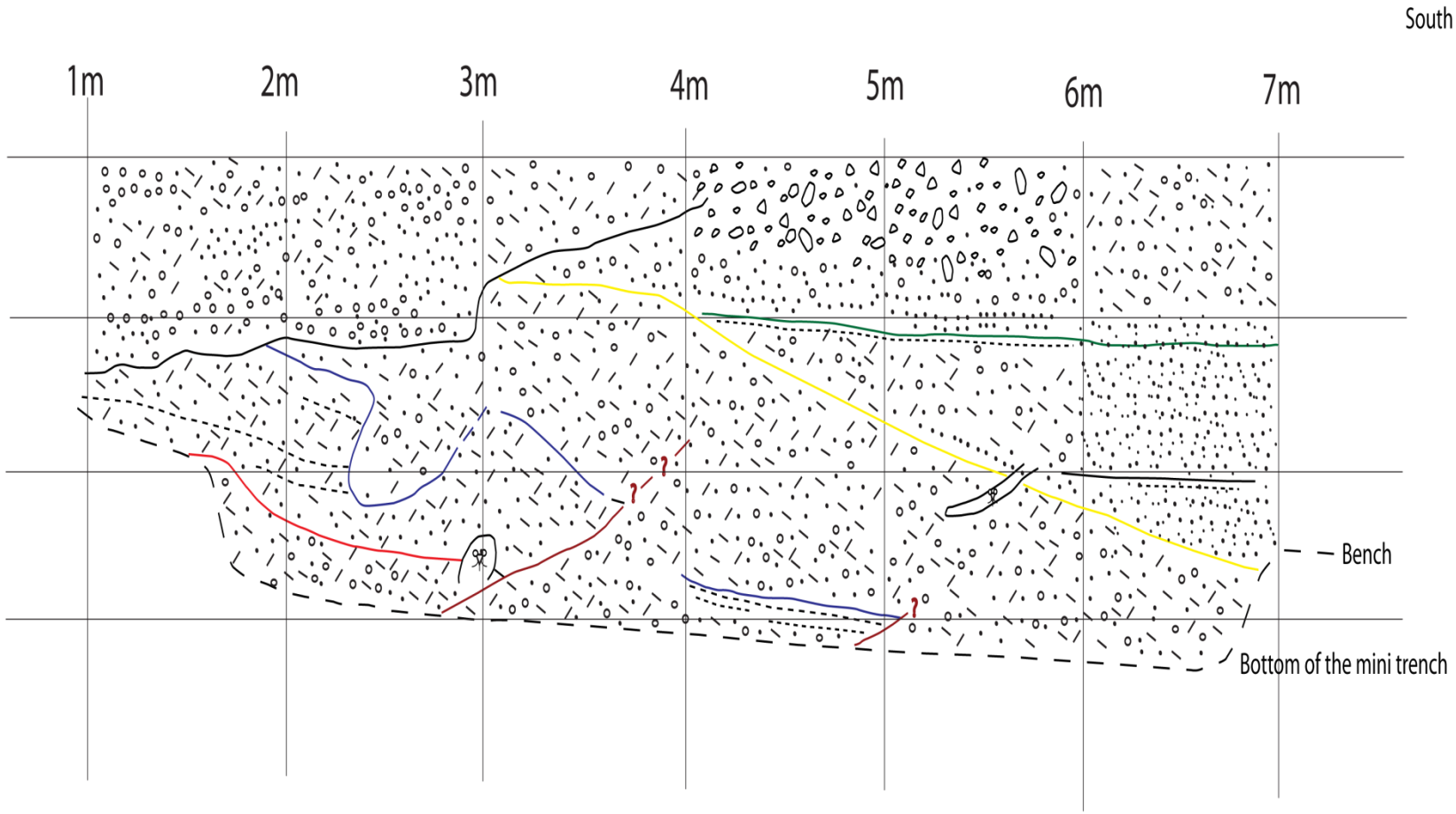

Figure A 1.2. Detailed log of north end of the east wall of Trench 5 (area shown in Figure 23), showing angular unconformity at base of Unit 400.

Figure A 1.3. Shows the potential fault tip in the east wall of Trench 5. (A) to (E) showing the step by step excavation to confirm the possible structure. In last figure (E) it proves that fault shape structure originally was a burrow.

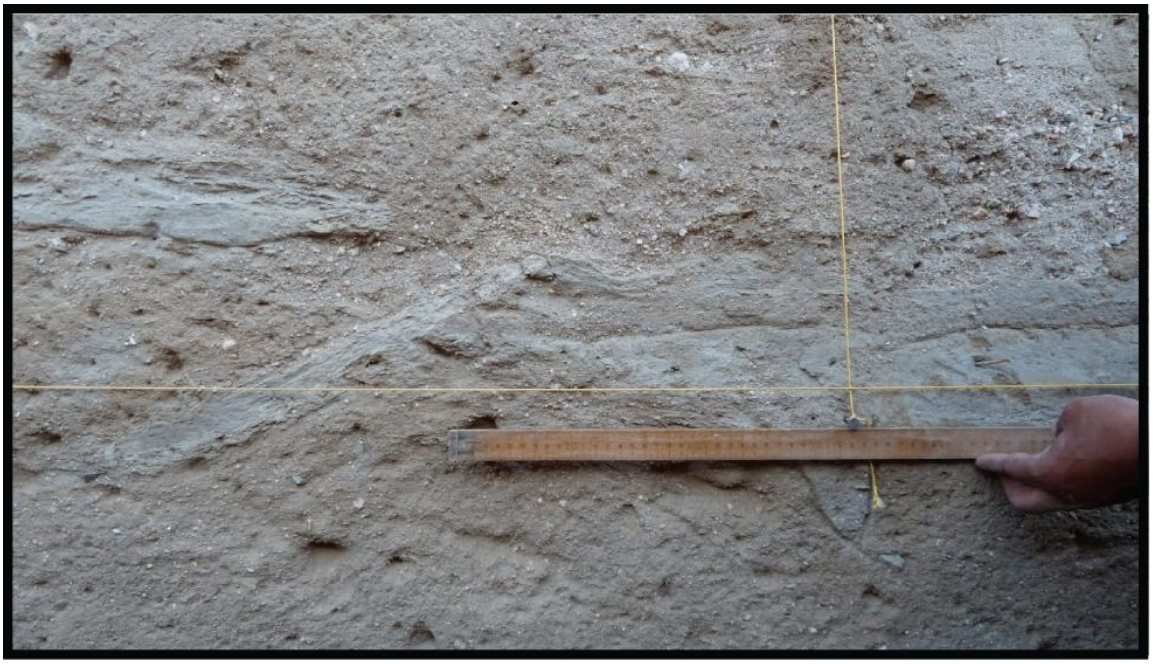

A) A long burrow in east wall between meters 5 and 6 cutting U4.

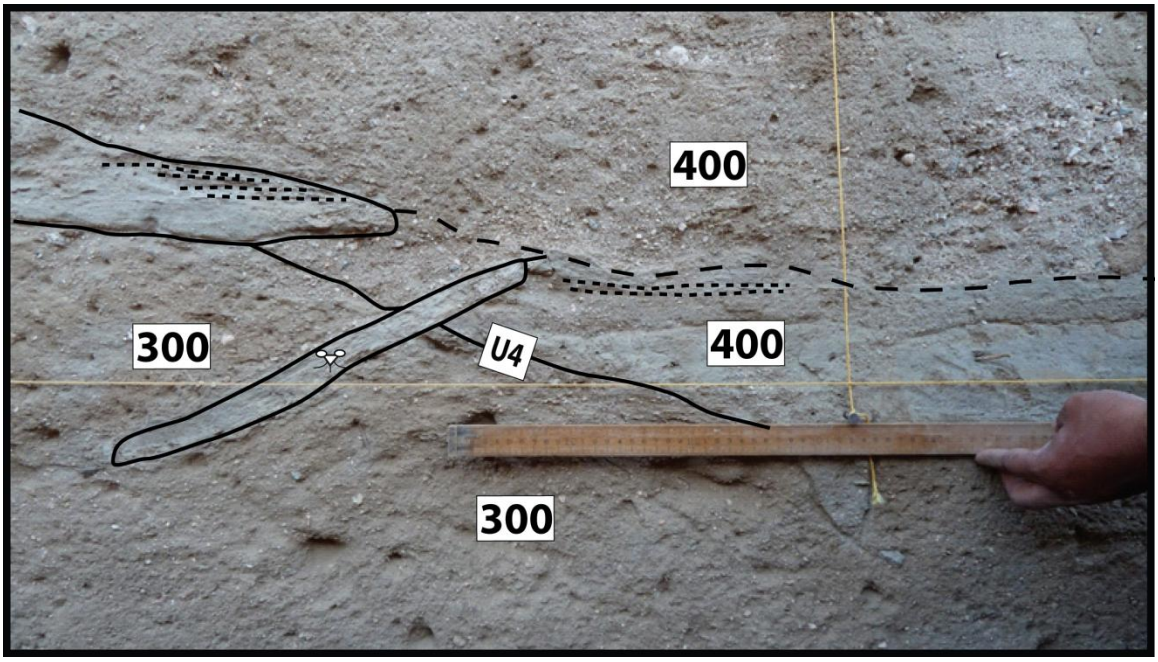

B) Photo shows s diagonal window which was dig out around burrow to find out exactly the length and width in order to correlate it with the structure.

C) Photo shows the view after the excavation of approximately 3 inches in east wall, burrow is almost disappearing. Burrows are outlined in black.

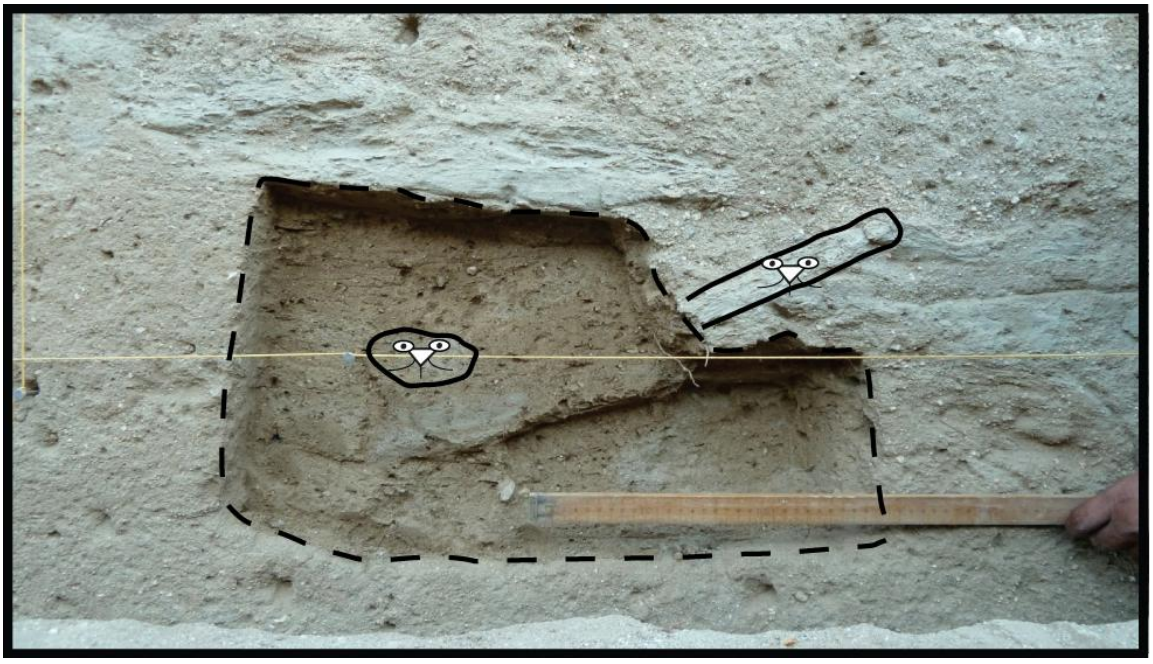

D) Photo shows the view after the complete excavation in east wall, burrow disappeared completely. Burrows are outlined in black.

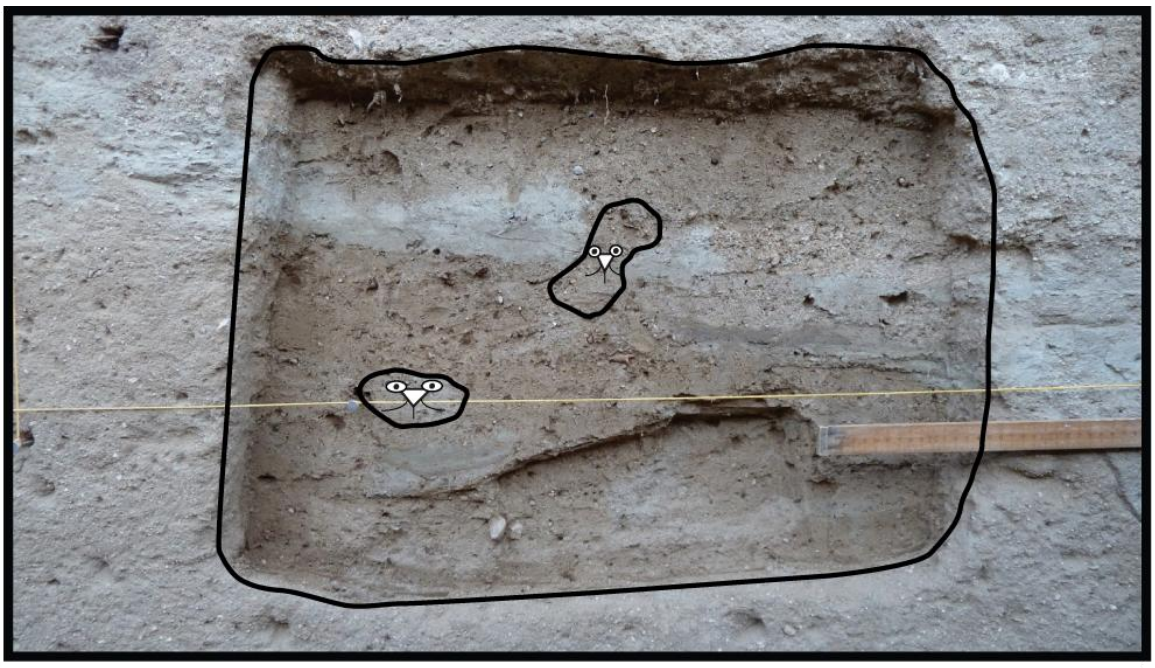

E) Photo shows the complete overview from meter 5 to 6, showing the clear continuity of U4.

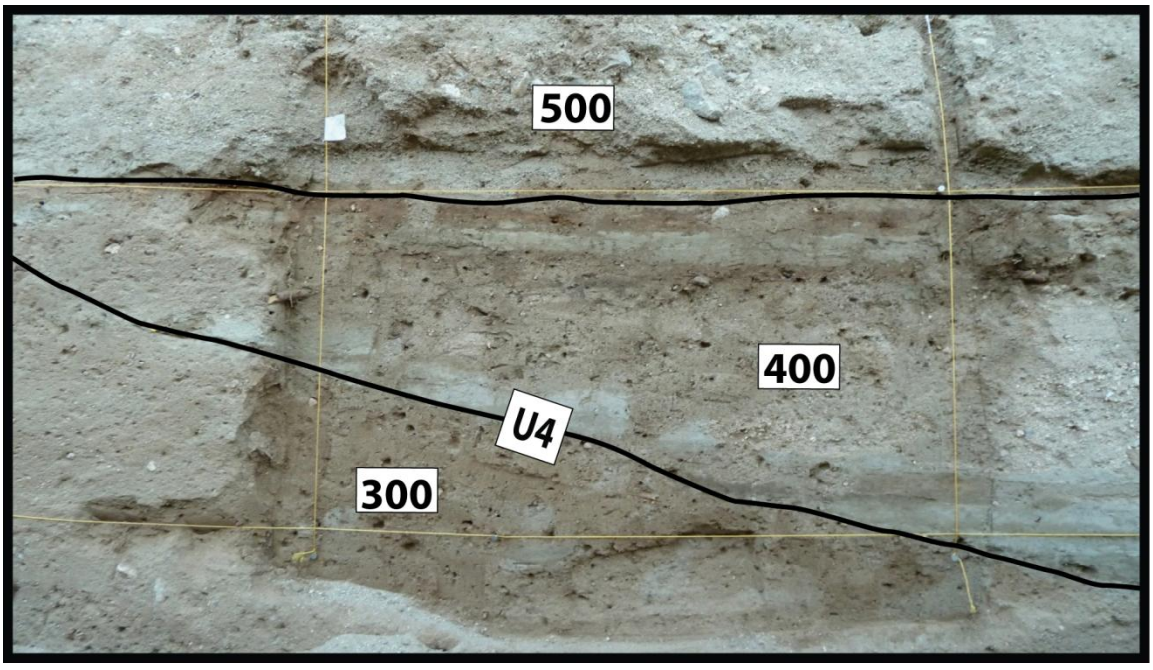

Appendix B

Five Optically Stimulated Luminescence samples were collected from west wall of Trench 5 by Katherine Kendrick of United States Geological Survey. The Optically Stimulated Luminescence samples were collected using steel tubes. After filling the steel tube with sediments, they were removed with care and sealed with aluminum foil and taped to prevent exposure to light. Optically Stimulated Luminescence samples were collected from the same units at the same levels as the charcoal to allow a comparison of the two techniques and to confirm the accuracy of the Optically Stimulated Luminescence ages. Optically Stimulated Luminescence samples are still under processing in the United States Geological Survey Luminescence Dating Laboratory (Denver, CO). Locations of Optically Stimulated Luminescence samples are shown in Appendix B.

Figure A 2.1. Katherine Kendrick (USGS) collecting an OSL sample 1 from massive sandy layer in Unit 200 (meter 17.5, west wall of Trench 5).

Figure A 2.2. Holes indicate locations of OSL sample 1 after collection from middle of Unit 300 at the 17.5 m mark of west wall of Trench 5 at depth of ~2.2 m below the ground surface.

Figure A 2.3. Holes indicate locations of OSL sample 2 after collection from top of Unit 100 at the 13 m mark of west wall of Trench 5 at depth of ~3.0 m below the ground surface.

Figure A 2.4. Holes indicate locations of OSL sample 3 after collection from middle of Unit 200 at the 12 m mark of west wall of Trench 5 at depth of ~2.7 m below the ground surface.

Figure A 2.5. Holes indicate locations of OSL sample 4 after collection from lower part of Unit 400 at the 22.2 m mark of west wall of Trench 5 at depth of ~1.5 m below the ground surface.

Figure A 2.6. Holes indicate locations of OSL sample 5 after collection from upper part of Unit 400 at the 20.6 m mark of west wall of Trench 5 at depth of ~1.2 m below the ground surface.

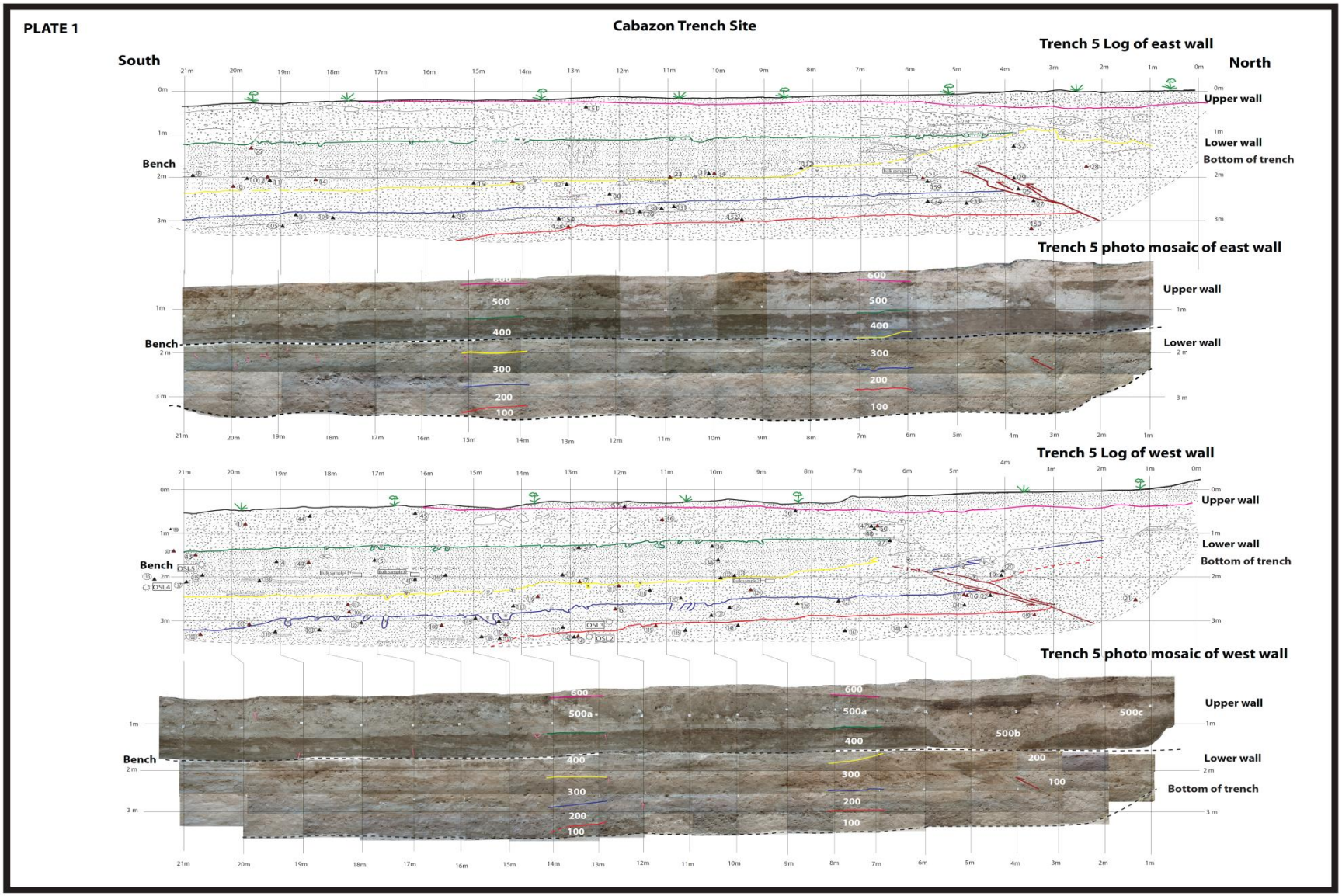
PLATE 1
Cabazon Trench Site
Trench 5 Log of east wall
South
North
Upper wall
Lower wall
Bottom of trench
Bench
Trench 5 photo mosaic of east wall
Upper wall
Lower wall
Bench
600
500
400
300
200
100
Trench 5 Log of west wall
Upper wall
Lower wall
Bottom of trench
Bench
Trench 5 photo mosaic of west wall
Upper wall
Lower wall
Bottom of trench
Bench
600
500a
500b
500c
400
300
200
100

PLATE 2

Cabazon Trench Site

Trench 6 Log of west wall

South

North

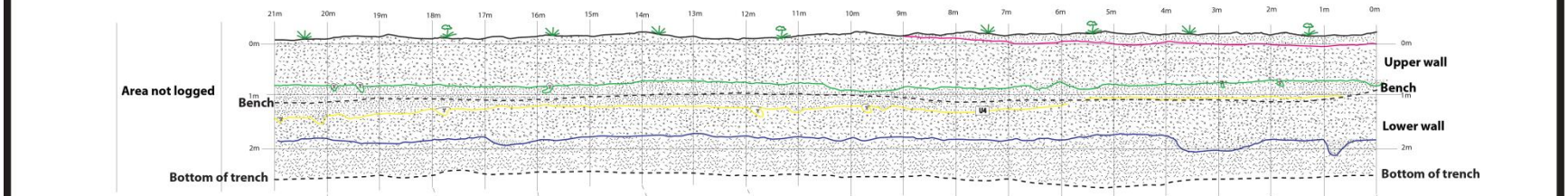

Trench 6 photomosaic of west wall

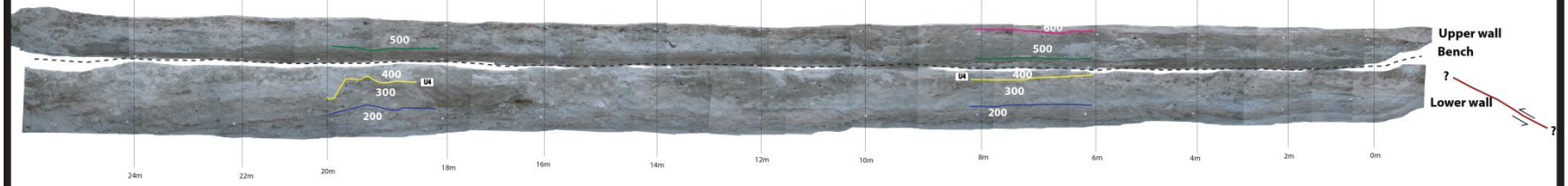

Explanation

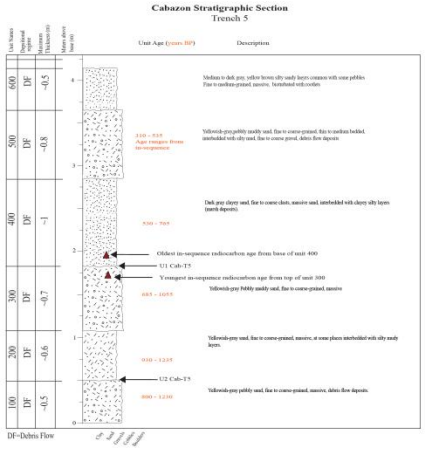

- OSL Sample locations taken by Katherin Kendrick of USGS.
- Locations of charcol samples collected and analyzed.
- Locations of charcol samples collected but not analyzed.
- Locations of bulk samples.
- Unconformities.
- Base or top of trench walls and bench locations between trench walls.
- Faults showing relative motion
- Burrows
- Ground surface
- Silty layers
- Massive sand unit
- Massive muddy sand unit
- Massive pebbly, muddy sand unit